UNIVERSITY OF CALIFORNIA SAN DIEGO

A Voice Coil Based Vibration Platform for Micro Robots Application

A thesis submitted in partial satisfaction of the
requirements for the degree
Master of Science

in

Engineering Sciences (Mechanical Engineering)

by

Mengxi Ren

Committee in charge:

Professor Nicholas G. Gravish, Chair
Professor John T. Hwang
Professor Tania Morimoto

2019

The thesis of Mengxi Ren is approved, and it is acceptable in quality and form for publication on microfilm and electronically:

_____

_____

_____

Chair

University of California San Diego

2019

TABLE OF CONTENTS

LIST OF FIGURES

ACKNOWLEDGEMENTS

First, I would like to thank my advisor Prof. Nicholas Gravish sincerely. I am grateful for the opportunity to work in his lab under instructions. This research project cannot be done without his valuable thoughts, continuously feedback, and long-term support.

I would also want to express my gratitude to the rest of my thesis committee members: Prof. Tania Morimoto and Prof. John T. Hwang for attending my thesis defense and giving feedback during the previous time.

Besides, I thank all the members of Gravish Lab for sharing their insights and experiences. It was warm having company from them, and there was a lot of fun working together.

Last but not least, I am grateful to my family for all the encouragement they gave to me throughout this project and their support for my staying at University of California, San Diego.

ABSTRACT OF THE THESIS

A Voice Coil Based Vibration Platform for Micro Robots Application

by

Mengxi Ren

Master of Science in Engineering Sciences (Mechanical Engineering)

University of California San Diego, 2019

Professor Nicholas G. Gravish, Chair

In micro-scale robot dynamics studies, there are still many challenges from their wide bandwidth, fast response, and high energy density properties. Among them, it is especially important to find a proper power source, and the piezoelectric actuator is the most popular solution. However, due to its intrinsic stiffness and friction, it brings complexity to the robot system. Since it is unnecessary for this kind of actuators to build an accurate model, we developed another power solution to substitute the traditional piezoelectric actuator. In this research, we fabricated and tested an experimental platform based on voice coil, which generates sinusoidal vibrations. We fixed a carbon fiber rod to a subwoofer with external constraints, including a Sarrus linkage. The Sarrus linkage was designed and built

using the SCM (Smart Composite Microstructures) method. With no feedback attended, the open loop system was proved to be able to generate accurate sinusoidal wave across 10-150 Hz. Integrated with a PI controller, the vibration platform was tested by giving a 1mm peak-to-peak amplitude output wave goal. Both the control voltage and output displacement were stable with smooth and fast transitions. To test the capacity, another loaded test has been done by attaching a compliant micro wing to the vibration platform. There is no significant difference between output displacements from loaded and no-load system, and all amplitude errors are smaller than 0.05mm. It is verified that this vibration platform is able to generate robust, accurate, and reliable sinusoidal wave at micro robot scale.

Chapter 1

Introduction

1.1 Research Problem

Nowadays, micro-scale robots became an increasingly important research topic. Working effectively in a limited environment, micro-robots have bright application potentials in scientific studies, disaster detection, surgical instrumenting, and extreme environment exploration. People have explored broadly in aerial [18, 14], near-ground [3, 1, 2], and underwater environments [27, 25, 9]. All kinds of movement including flapping, undulatory, and vibration have been realized in micro-scale robots. It is an obvious trend that micro-robots were commonly inspired by insects and small agile animals, e.g., inchworm [23], earthworm [15], flea [8], fruit fly, and bee [19]. Also, it's not hard to find that typical characteristics of those animal prototypes are their high-speed locomotion, fast response, and high energy density's actuation. Those impressive biological abilities help small animals to accelerate, turn, and stop fast in chasing prey and escaping from predators. However, it brings a challenge to microrobot design and fabrication. Delicate mechanisms design and proper energy source have to be developed to maintain microrobot's agility and strength.

For the power source, the most popular choice so far is the piezoelectric actuator

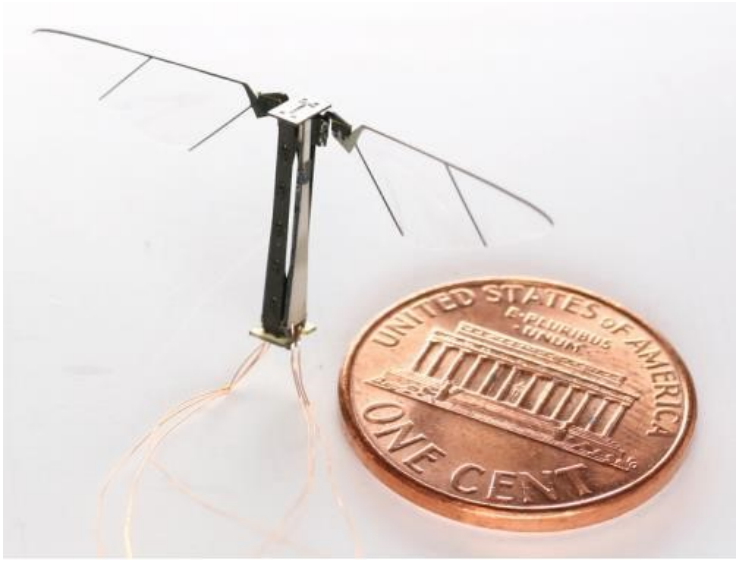

Figure 1.1: the Harvard Robobee [20]

[23, 26]. It has been used in aerial, near ground and underwater experiments. The reason for the preference is because of the material's long lifetime, stability, high power density, and customizable size. This kind of actuator can provide accurate, high bandwidth, and controllable force. Based on that, many Interdisciplinary studies have been carried out to better understand the dynamics and mechanisms of bio-inspired microrobot systems. Take the RoboBee [20] from Harvard as an example, it is a bee-like micro aerial vehicle with 2DOF [20] or 3DOF [19]. It is important to study the onboard capacity from the energy aspect, and many studies have discussed the optimal choice from the wing and transmission aspects [13]. However, if we continue the research and aim to explore more deeply, we need to face the dynamics influence from the actuators. As is shown in 1.2, we built a dynamics model in Matlab Simulink to simulate the flapping-wing system. After importing all the real parameters as in the real micro-robot system(shown in the right side), we did a frequency sweep and an amplitude sweep. That is, we fixed the control frequency, and ramp the control amplitude up. The result is shown in 1.3. As we can see from the result comparison, the resonant performances are not all fit well at different frequencies.

This simulation model is realized not reliable enough. Since piezoelectric materials have an intrinsic stiffness [4], it plays an important role in whole system dynamics, and we didn't consider the actuator's stiffness in the dynamics model we built. Since there is no simple and straightforward modeling of hand-made piezoelectric actuators, it makes it hard to model the robot system completely.

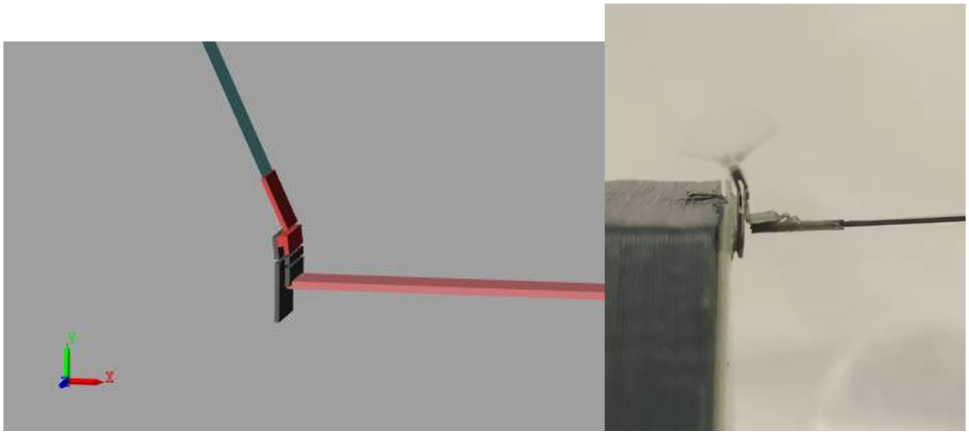

Figure 1.2: A comparison between Simscape animation and the real flapping-wing system

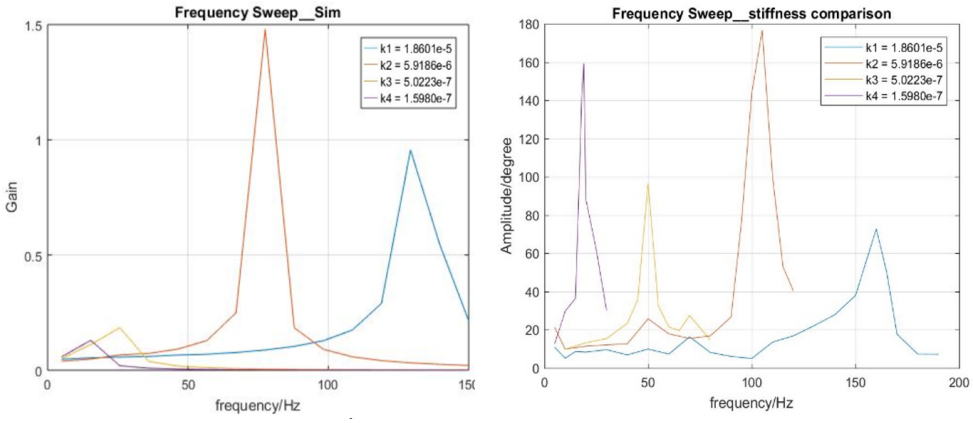

Figure 1.3: The comparison between frequency sweep test result in simulation and real system

Thus, although it is proved practical to use piezoelectric actuators in micro-robots, we can not get to avoid the difficulties of dynamics modeling easily when we are trying

to find an optimal solution. To get rid of this, we can separate the research process into two parts. We can build a stable, reliable, and relatively large power source to actuate the robot system, in another word, to simulate the actuating scenes. When the big actuating platform is robust enough, the actuator's dynamics influence could be ignored. After the optimal solution of the system without the actuator is found, we can integrate the original actuator back to the system, and make the solution. This two-steps method can minimize a complicated system's dynamics and can save much cost.

In this work, we discussed an actuating platform solution. We propose a reliable linear sinusoidal motion generating system, which is stable, long lifetime, cheap, and easy-to-fabricate. Based on a subwoofer, the platform can generate pure vertical motion. Including a Sarrus linkage, a set of external constraints has been built to cancel the horizontal movement. Although the woofer-shaker is already sturdy enough to cancel robot dynamics influence, the open-loop control based on empirical test results cannot provide the required high-quality vibration. Thus, we realized a closed loop displacement control with an embedded hall effect sensor along with a small magnet. With the active control, the platform can generate steady, high resolution sinusoidal vertical vibration. Although the platform itself is not able to be assembled into a micro robot due to weight and size limitation, it can be used as a general power source in testing when the system is too complicated to explore.

Chapter 2 gives a brief introduction to voice coil actuators. Comparison between traditional piezo-actuator, commercial voice coil motor, and the subwoofer-based shaker has been discussed.

Chapter 3 introduces the system design and fabrication. Along with sketches, it gives an introduction of mechanical design including the woofer base, the holding carbon fiber rod, the rod fixture, and the Sarrus linkage as a horizontal constraint. It also discusses the materials and method used in building the system. Chapter 4 explains the control

algorithms used in the closed loop feedback system. Working with a hall effect sensor to detect the rod position, a PI control have been embedded in the platform. It assures the system to have a stable, proper, and controllable vibration output.

Chapter 5 is the experimental testing. A curve fitting of the hall effect sensor calibration has been given. Both open loop and closed-loop control's results have been discussed. Also, we attached several loads to the system to mimic the real testing environment, the shaker is proved to be reliable to give steady sinusoidal vibration.

Chapter 6 gives a summary of the work done in this thesis. It also suggests future work in potential research areas.

1.2 State of the art in micro linear actuator

For the increasingly high needs in optical, semiconductor, and aerospace industries, people have been explored a lot from different aspects to develop high-resolution positioning devices. Among these studies, piezoelectric materials are one of the most popular choices. Initial piezoelectric (PZT) actuators have great positioning accuracy of nano-scale, but its stroke distance is usually short due to the material's intrinsic stiff properties [26].

Some PZT-driven actuators have relatively long working distances and high resolution at nano-scale. In Ronan Le Letty et al. 's work [17], they introduced a linear piezo-motor which has a positioning accuracy of 0.1 μm, a maximum driving force of 17N/37N and a maximum stroke of 10 mm. However, their motor's speed was at 55/23 mm/s, which cannot realize an accurate vibration with 1mm stroke at 150Hz. Jaehwan Kim et al. developed a hybrid linear actuator based on stacked piezoelectric actuators and two clamping devices [16], which has a maximum blocked force of 0.9 kg. However, neither the travel distance or the driving speed is big enough to satisfy industrial needs. Some other kinds of PZT-driven actuators used precise actuating shaft mechanisms to achieve

several millimeters travel distances, but they usually lack repeatability due to backlash and friction.

Except piezoelectric actuating, conventional voice coil motors have been used in building high precision positioning systems. Shigeri Mori et al. [22] first studied the performances of an air-bearing linear actuator in HDD(hard disk drives), pointed out the candidacy of this system in high precision positioning needs. It has a wide bandwidth extended to 4kHz and a high resolution of 0.5 nm. They later improved the NMA(nano-motion actuator) to achieve a larger working distance of over 50 μm and proved the positioning stability [21].. Although the actuator's resonant frequency is considerably high to give a large bandwidth, the working distance is still relatively small.

Also, Magnetic levitation has been used to assist existed micro linear actuators. Christine Ruffert et al. [24] introduced a method to utilize and fabricate a magnetic guide system as a linear actuator. With a nearly frictionless solution, the motor's response speed and accuracy are promising. However, the system has a load capacity of only 10 mN, the robustness of the system is not proved either.

1.2.1 Introduction to thesis topic and method

The solution to a reliable, stable, and high-resolution linear actuating power source is not currently off-the-shelf, and it's usually unnecessary to spend too much cost of building a testing platform. Thus, it is meaningful to develop a cheap and practical actuation solution, through which people can benefit more in micro-robots studies, optical calibrations, and high precision experiments. In this work, we have developed a subwoofer-based vibration generating platform, which can substitute traditional micro robot actuators in testing needs. Laser cut and lamination method have been used to build the platform.

Chapter 2

Voice Coil Actuators

2.1 Why subwoofer-based actuator?

In order to find a satisfying power solution, different methods have been attempted.

The first thought was to design or find a proper piezoelectric actuator. This kind of actuators work based on piezoelectric materials, has great advantages of high power density, lightweight, accurate, high-frequency response. There have been studies between whether the motor and the piezoelectric actuator has the ability to drive micro flapping-wing robots [7]. However, it is most likely that a robot system has complicated dynamics model. Although there are some studies about piezoelectric actuator's dynamic modeling [6], it cost both time, calculation memory, and fabrication cost. Considering the need for micro robot system integration, commercial piezoelectric actuators are too modular that it can't satisfied flexible design/prototype requirements. A traditional way to integrate this actuator to micro-robots is to build it in a lamination way, and that brings more drawbacks to dynamics calculation due to fabrication offset and manual operation error.

Thus, we changed our mind from the existed, common-used power solution to a more general device for testing use. In this device/ platform, we hoped to generate accurate,

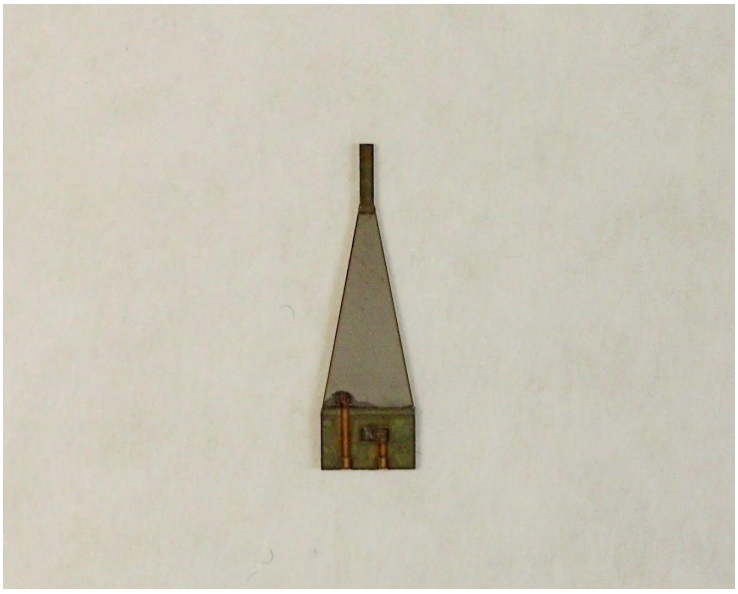

Figure 2.1: A piezoelectric actuator

stable, and controllable signals. After attaching the actuated part, the system can simulate the microrobot dynamics. The most crucial point of this method is, the actuator's output vibration has to be strong and robust, which won't be influenced by micro robot scale's dynamics. Based on that idea, we looked into voice coil motors for its excellent performance in the frequency needed (100Hz). Shown as the picture in figure 2.2, we found a commercial linear voice coil motor [11] with embedded encoder. The accurate high-frequency vibration requires the encoder's high sensitivity. Take our previous micro flapping wing robot as an example, the piezo-actuator's tip distortion is around 2mm peak to peak. Assume a 100 points per cycle's sinusoidal wave is precise enough, the maximum resolution is. This motor we chose has a 1.25 microns resolution, which seems enough for our working need. However, there were several issues that appeared in our experiments. As the figures showed below, the displacement data started to randomly drift when frequency increased. We ended up an explanation that this encoder was not designed for reading from vibration, but specific position reaching. To find an affordable commercial voice coil motor, which has both high resolution and a fast response encoder was difficult.

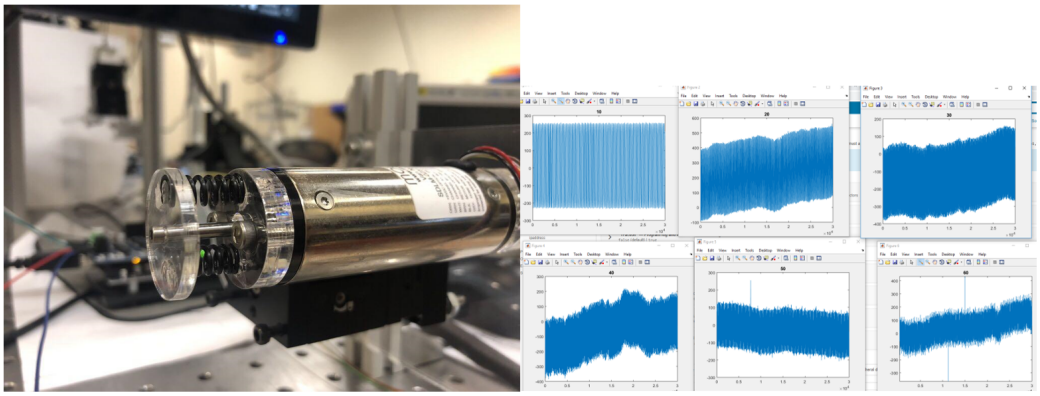

Figure 2.2: A voice coil motor

However, the idea of using the voice coil was instructive. Due to the working properties, a voice coil based setup's response is fast and stable. As a subwoofer's working frequency range is below 300Hz [5], it should have a satisfying performance in a micro flapping wing robot which works around 150Hz [19]. We looked through speakers in the market, chose this subwoofer to be the design basis. There are several advantages for using a subwoofer as the actuating source. In the mature audio industry, we can easily find products datasheets and figure out the working range. The mass of a subwoofer is way more than that in microrobots, and the impedance is also big enough to support the robust power source. Although there is no embedded encoder to show its performance, we can also integrate a displacement sensor into the system. Moreover, in that case, the sensor's selection could be more flexible and practical. Overall, the choice of using a subwoofer as the power source is cheaper, more accurate, and more reliable. We will introduce more details of "using a subwoofer as actuating source" later in the next section.

2.2 Working principle of subwoofers

A subwoofer, or in general a speaker, works according to the figure shown below. The 'S', 'N', 'S' shows a permanent magnet. A metal coil sits in front of the permanent

magnetic, which is fed with electricity. For the coil, an important property of it is that it can be considered as a temporary electro-magnet when electricity passed through it. Thus, when we feed electrical signals to the coil through the cables attached, the polarity of the will follows the current direction. This change of voice coil direction will pull the cone back and forth as needed, then the cone's vibration will generate sounds and diffuse it to the air. In our design, the outer cone part is considered unnecessary since we don't need the real enlarged sound. Instead, a large volume sound will influence the air dynamics around, and bring unnecessary chaos to the system tested. We took most of the cone off, used the bottom section as the vibration source.

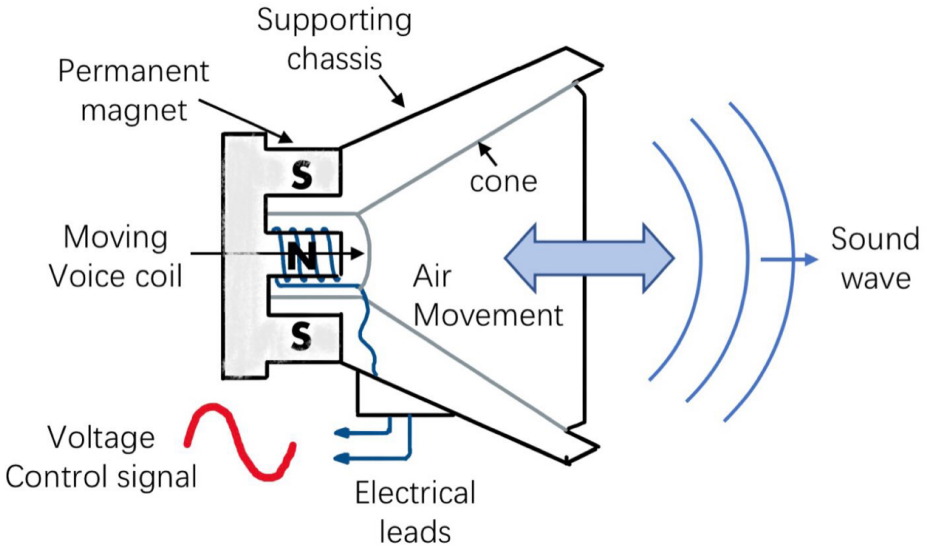

Figure 2.3: The Working principle of a subwoofer

2.3 Wiring and control flow

As is shown in the block diagram below, the workflow of this system is straightforward. The PC software interface is the main role of the system control, which reads measured

data, realize the closed-loop control, and generates the control signal. A data acquisition device works as the hardware port, connects the vibration platform (through a voltage amplifier) and the connector. The vibration generated by the platform, as the system output, is measured by a displacement sensor. The measured data is used as feedback in the closed-loop control system.

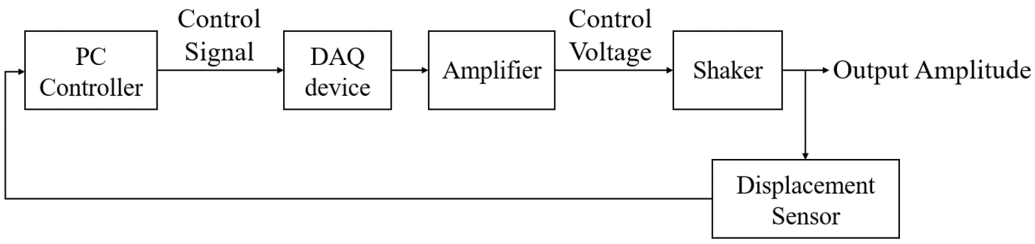

Figure 2.4: Electrical wiring of the system

Chapter 3

Subwoofer-based Vibrator and the Fabrication

3.1 Design sketch of the vibrator

In this chapter, we will discuss the mechanical design and fabrication of the subwoofer-based vibrator. Materials, fabrication methods, and fabrication equipment have been used will be introduced.

Figure 3.1 is a design sketch of the system. The major parts are a subwoofer, a carbon fiber rod, an acrylic fixture board, and a Sarrus linkage. We found a subwoofer in the market fit the calculation requirements; it works as the power source. The carbon fiber rod is attached to the inner voice coil, it moves up and down along with the voice coil. As a connector, it will be attached to the robot system when doing experiments. To ensure the vertical motion, an acrylic board constraint and a Sarrus linkage are integrated into the system. A PC control interface is developed to give the control signal, and an amplifier is also needed to provide enough control voltage.

We will discuss more details about design ideas and fabrication methods for each

part in the following sections.

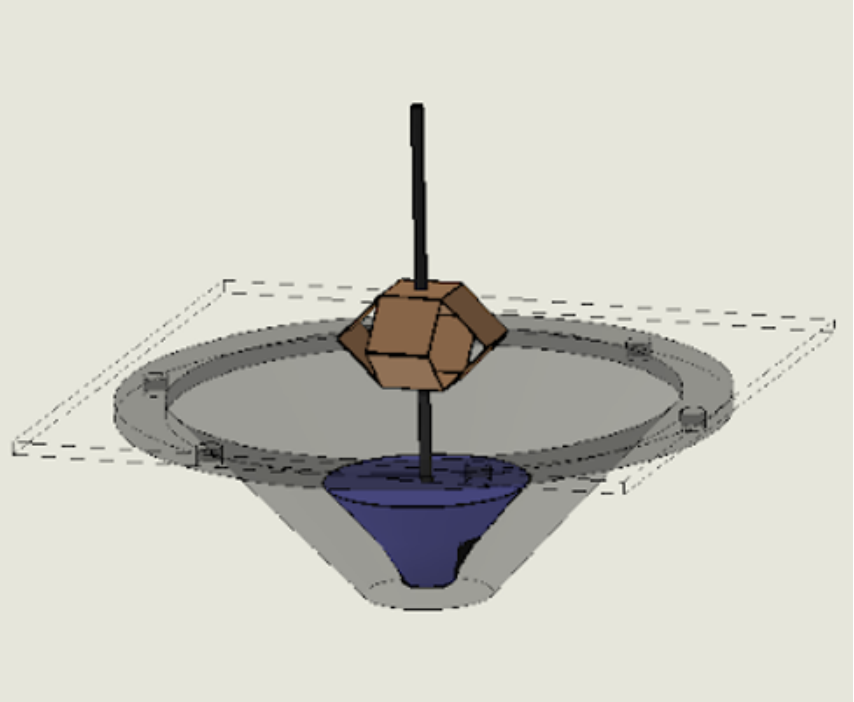

Figure 3.1: Design sketch

3.1.1 membrane cut

First, to decrease the unnecessary enlarged vibration and make the system easier to assemble, we need to cut peripheral cone. As is shown in figure 3.2, the surface membrane and most section of the cone are removed. The metal cone, connected to the yellow part, is the voice coil which moves up and down as controlled. We can also see that there are two electricity ports, which intend to extend the functions of the system. The voice coil and the wiring points are the most important parts from the original subwoofer, so we need to cut the membrane carefully.

Figure 3.2: the membrane Cut

3.1.2 carbon fiber rod fixture

Next, we need to attach a carbon fiber rod to the voice coil vertically. The carbon fiber will work as the connecting element between the vibration generating platform, and the robot system need to be actuated. The carbon fiber fixture's design idea is shown in figure 3.1.

First, we glued an FR4 plate (with a 0.3mm thickness) on the top of the moving voice coil. As no part has been directly removed from the voice coil cone top, we consider the FR4 plate flat and horizontal, and it will be the bottom plate to fix the carbon fiber rod. As we hope to develop a vibration generator which could provide pure vertical sinusoidal wave, it is extremely important to cancel the horizontal move. This motion is mainly from the operation error when we glue the FR4 plate and the carbon fiber manually. To reduce it, two external constraints in the horizontal direction have been applied.

We design and cut an acrylic board, which has a center hole and can be fixed solidly to the subwoofer chassis. The center hole is designed to have the same radius as the carbon fiber rod, but it's slightly larger than carbon fiber due to laser fabrication. Then we put the carbon fiber rod vertically through the hole, stick it to the FR4 plate. Before the glue settled down, we manually adjusted the carbon fiber angle by some vertical motion test. The carbon fiber rod cannot achieve a satisfying vertical motion, for there is some free

space between it and the constraint hole. From high-speed videos, we can find the "loop" track of the motion. To improve that, another constraint called Sarrus linkage has been added.

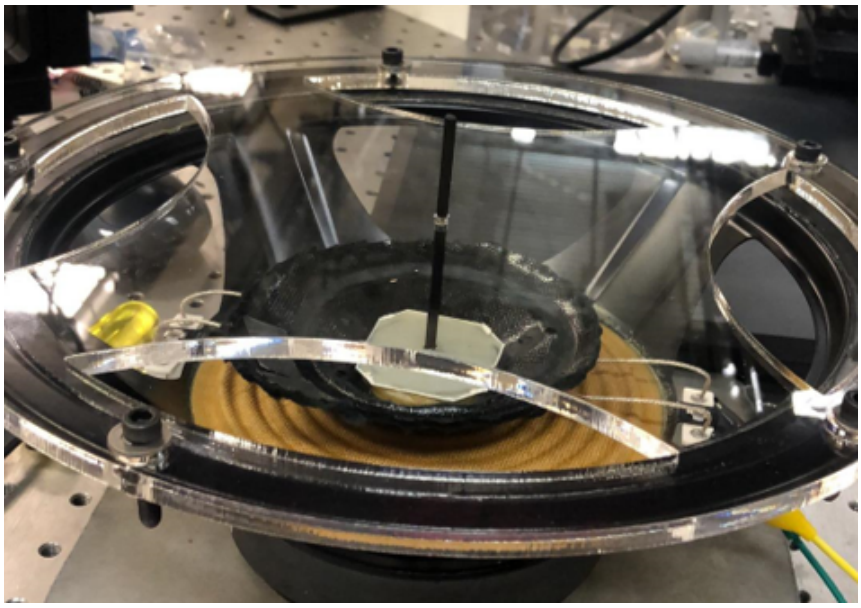

Figure 3.3: the carbon fiber rod fixture

3.1.3 Sarrus Linkage

Sarrus linkage is a mechanical linkage to convert limited circular motion to linear motion or vice versa without reference guideways[30]. It has four links in two identical groups that are perpendicular to each other, with all links having equal lengths. The top plate moves up and down relative to the bottom plate. Those connecting hinges work to push or drag the top plate to remain at the same level as the bottom plate. Although it is usually used to convert circular motion to linear motion, its mechanisms determine that it can also work as a linear constraint.

In our design, there is a Sarrus linkage with its bottom plate fixed to the acrylic board/subwoofer chassis and a top plate fixed to the carbon fiber rod. As is shown in figure 3.3, blue triangles are fixpoints. Considering the hinges forces explanation above,

the top plate and the bottom plate can only move parallelly. Therefore, the Sarrus linkage constrains the rod's horizontal drifting, the carbon fiber rod's motion turned to be pure vertical as needed.

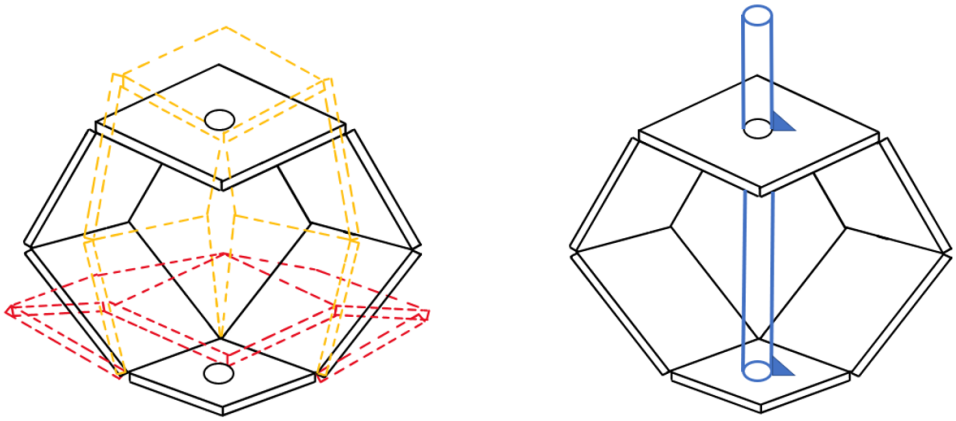

Figure 3.4: Working principle of a sarrus linkage

3.1.4 Electrical Wiring

The electrical wiring idea of the vibration platform is quite straightforward. A PC software interface at the outer control terminal records the motion goal (vibration frequency, amplitude, resolution, etc.) by manually input and produce control signals by calculation. A DAQ (data acquisition) device provides voltage control signals and reads the feedback signals from the displacement sensor. Because the DAQ device is incapable of providing enough power to actuate shaker, an audio amplifier works to enlarge the control voltage signal. Fed by the amplified voltage signal, the shaker generates controllable vibration. An embedded displacement sensor measures the output vibration and sends the data back to PC calculation via the DAQ device.

3.2 Fabrication

3.2.1 Equipment used

There are mainly two instruments being used in this system fabrication. Âů Laser Machines (a commercial Glowforge laser machine and a high precision laser machine) Âů Hydraulic Presser

The Laser Machines

A commercial Glowforge laser machine has been utilized to cut the acrylic constraint board and to prototype the Sarrus linkage. Glowforge Plus [10], the powerful laser machine has the functions of autofocusing and 3D engraving with onboard cameras and remote operations. The materials compatible with the device include wood, leather, acrylic, fabric, cardboard, and paper.

Although some materials (FR4, Adhesive Film and Kapton Film) used in the fabrication are not standard, and there are not any reference operation parameters, the laser machine did a great job to cut through those materials.

Also, a high precision laser machine has been used to fabricate the microrobot parts. It's a lab-assembled laser machine, with a maximum average power of about 2W. The most common applications for this laser machine are micro robot fabrication and micro 3D depth engraving. Materials have been tested to compatible with this laser machine include PZT ceramics, ferrite, stainless steel, brass, copper, nickel, nitinol, polyimide, thin polyester, carbon fiber prepreg, glass fiber prepreg and Kapton (ref shivam thesis). Compares to the Glowforge laser machine, the working range of this laser machine is much smaller so it can't be used to cut large setup parts. However, it has impressive cutting resolution with sufficient power. Therefore it's no doubt the satisfied solution for microrobot fabrication.

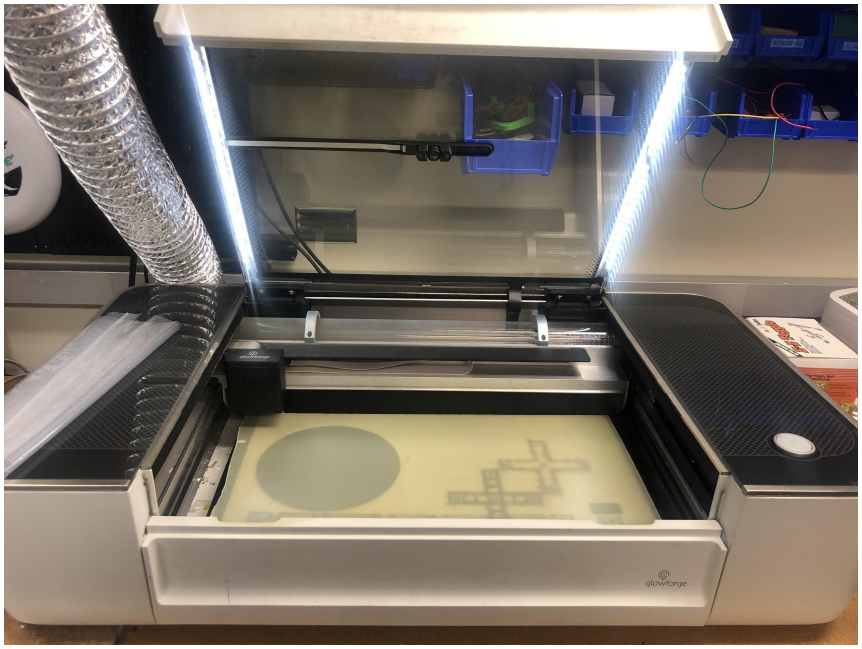

Figure 3.5: The Glowforge laser machine

The Hydraulic Presser

We are using adhesive material for both the Sarrus linkage and the micro flapping wing, and this material is pressure sensitive. Thus, to implement the lamination press, a hydraulic presser has been used to do the composite materials pressing.

A 2000 lbs pressure has been applied to the Sarrus linkage composite lamination for 30 minutes, and a 300 lbs pressure has been applied to the micro wings for 20 minutes. The wings were all excellent with nothing broke apart in tests, as same as the Sarrus linkage.

3.2.2 Material

As in the pictures below, a subwoofer from Dayton and an audio amplifier from BOSS have been used in the shaker fabrication and tests. The 10' DVC subwoofer has a wide frequency response range up to 2000Hz, which is sufficient for out micro robot application (usually lower than 1000Hz). Also, the 6mm maximum linear excursion is way larger than the conventional PZT actuator's tip displacement (<3mm). Accordingly, we

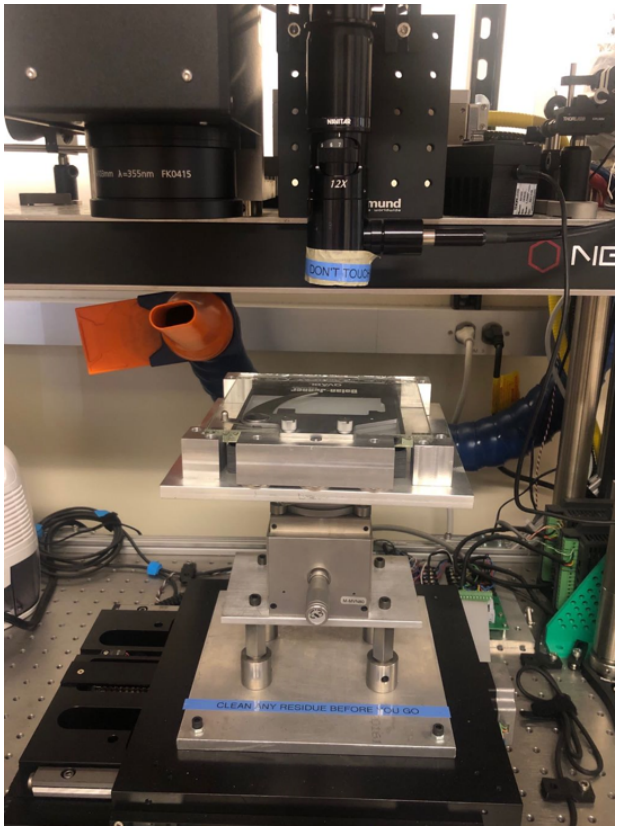

Figure 3.6: The high precision laser machine

chose a 1200-Watt, 2 channel amplifier for this subwoofer.

A carbon fiber rod with 0.25mm radius is used as the supporting/connecting rod. It also works as a displacement indicator to check the shaker's performance.

As the fundamental main parts in pop-up design, film materials are undoubtedly important in the design and fabrication stages. The thickness, stiffness, strength, extensibility, lifetime, heat, and vibration resistance of each layer determine the composite structure's mechanics and dynamics properties. Some typical film materials we used are carbon fiber composite film, Kapton, FR-4, and adhesive layer.

FR-4 is a composite material composed of woven fiberglass cloth with an epoxy resin binder that is flame resistant(ref wiki FR4) [28]. This material's mechanical properties are directional oriented, and there are distinct strength and stiffness differences between the

Figure 3.7: The hydraulic presser

fiber direction and the cross-section. However, the fibers are thicker compares, and this material is considered to be strong compares to the other films. Thus, it's often used as supporting materials in chassis/ skeleton.

Kapton is a polyimide film which has stable mechanical properties across a wide range of temperatures (from -269 to +400 C [29]). This material has isotropic mechanical properties, has good temperature stability and long lifetime under vibration. With different thickness levels, the stiffness of Kapton could vary a lot. Thus, it's commonly used as the joints in micro-robot fabrication with customized shape and stiffness.

Adhesive film materials are the connecting parts in lamination fabrication. Layers of different functionalities need to be fixed together by adhesion. There are several types of adhesive films, e.g., pressure sensitive one and heat sensitive one, and researchers usually

Figure 3.8: The subwoofer: SD270A-88 10" DVC Subwoofer 4Ohm, Dayton Audio

Figure 3.9: The amplifier: R6002 RIOT 1200 Watt 2 Channel MOSFET Car Audio Amplifier, BOSS

choose the material depends on the need. In this research, we choose the pressure sensitive one due to the relatively big working area of the Sarrus linkage.

For the Sarrus linkage, we have used the following films:

FR-4

Pressure Sensitive Adhesive Layer

Kapton

For the micro wings, we have used the following films:

Carbon fiber film (3 prepregs pressed as 0-90-0)

Pressure Sensitive Adhesive Layer

Kapton 30, 50, 100

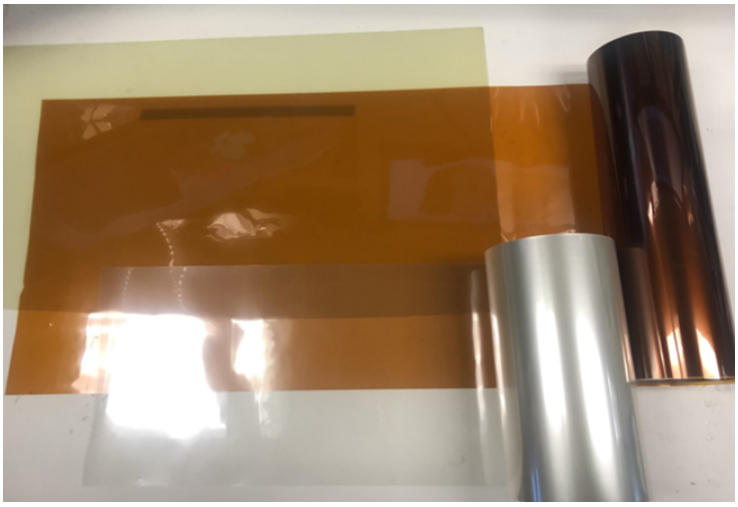

Figure 3.10: The film materials used

3.2.3 Method in building the Sarrus linkage

To build the Sarrus linkage, we used pop-up design and the lamination method to fabricate. It's also called Smart Composite Microstructures (SCM) as shown in fig 11.

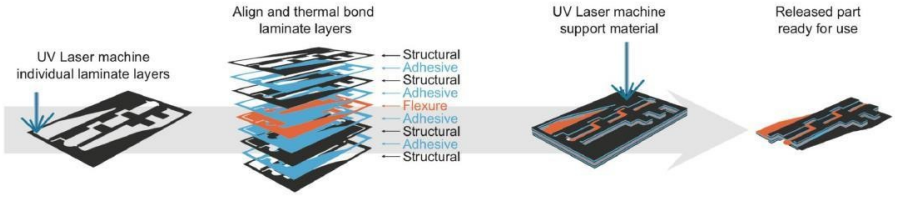

Figure 3.11: SCM(smart composite microstructures) method

Overall, the lamination method is to manufacture a prototype by pressing multiple layers, so the composite material/structure has better strength or stability or other properties performance. A release cut should be done after the press, to take the composite material out and to finish later necessary assemble. Each layer should be designed specifically to realize the design goal of a complicated composite structure. It's usually a "sandwich" structure, which has strong outer layers as the supporting chassis, temperature or pressure sensitive adhesive layers to connect component layers together, and flexible layers to be the soft joints. Sometimes In complicated micro-part, pre-cut should be

considered in the design to prevent potential spatial conflict.

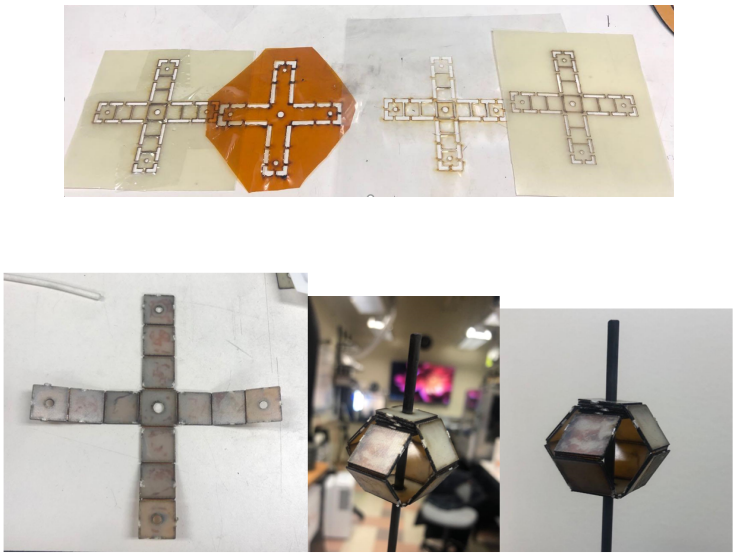

Figure 3.12: Fabrication of the Sarrus linkage

Figure 3.12 shows each layer of the Sarrus linkage(FR4 - Adhesive - Kapton - Adhesive - FR4) and the composite prototype after release and assemble. The linkage is around 15mm 3 big and could fit the carbon fiber rod through the center hole.

Figure 3.13 shows each layer(Carbon Fiber - Adhesive - Kapton - Adhesive - Carbon fiber) and the final prototypes of the micro wings. There are four wings in one bunch of wings lamination. Notice that to explore different wing stiffness levels, we made different hinge width with different kinds of Kapton. According to the stiffness calculation(calculation formula here), the wing stiffness increases from the left to the right in figure 3.14.

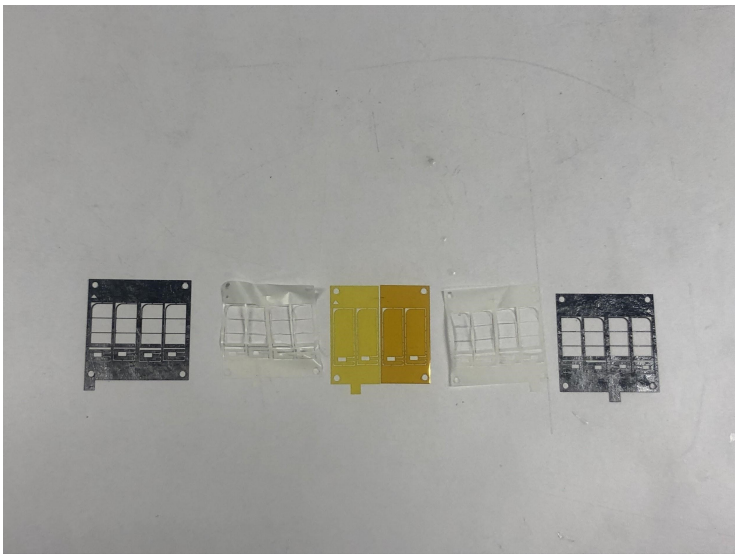

Figure 3.13: The layers used in micro wings fabrication

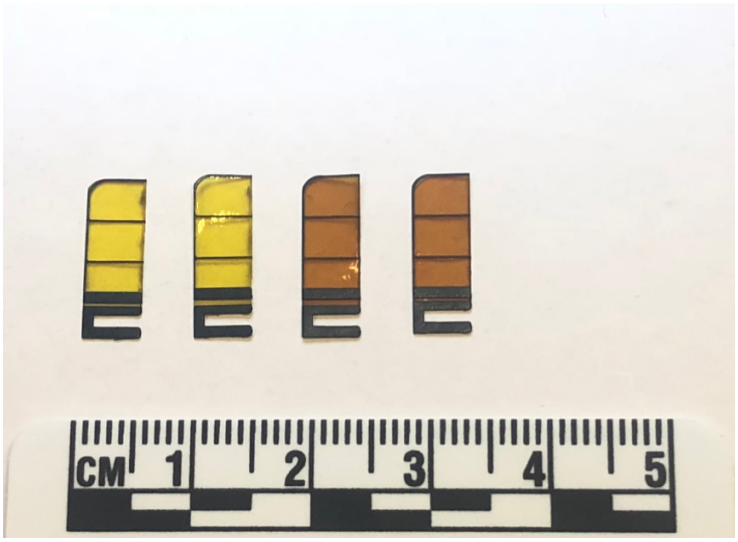

Figure 3.14: The micro wings prototype

Chapter 4

Closed-Loop Control Algorithms

4.1 Introduction to general PID control

A PID (proportional-integral-derivative) controller, is one of the most popular choices in the industrial control system. This controller continuously works to calculate the error between a setpoint and the measured output value using, calculates a control correction using proportional gain, integral gain, and derivative gain.

In a PID model, P gain is used to reflect the difference proportionally. For example, if the error between the setpoint and measured value is large, the control correction from P gain will be proportionally large, which depends on the gain value Kp.

I gain is used to reflect the difference integrally. It is usually used to eliminate the residual error after the P controller applied. By adding an integral gain Ki, the historic cumulative error will be taken into account and make feedback on the control correction.

D gain, as the derivate gain, can decrease the settling time and increase the stability. Based on the current measured error changing rate, it works to estimate future error changing trend and contributes to control correction.

However, although a complete PID controller works fast, strong and accurate, it

costs a lot in parameters tuning, and sometimes the complexity and possibility turned to be too tough to find a satisfying solution due to some intrinsic drawbacks from either the P or I or D term. Thus, a perfect PID controller is sometimes unpractical.

4.2 Reason for choosing PI control

Now since the PID controller is supposed to be overkill, what is the difference between P / PI / PD or other combination controllers and which one do we prefer? The first thing we need to notice is that the P term is necessary for all kinds of controllers. The reasons are simple: the proportional control is the fastest, concise, and straightforward approach to reach our system's output to the desired goal. Neither I term, or D term works as fast and effectively as P term.

However, if there's only proportional control, and when the control gain Kp is too large, it brings oscillations and the steady-state error. The PI controller and the PD controller are common solutions. For PI controllers, they cancel the steady-state error, decreases the amplitude of overshoot. However, they are not working effectively when the controlled variable is slowly changing. For PD controllers, they are more stable, and they decrease the settling time. However, PD controllers can't remove steady-state errors, and their performances are seriously influenced by high-frequency noises.

In this research problem, the controlled variable is a fixed vibration amplitude across a relatively broad range of frequencies, and it needs to be really accurate that the steady-state error has to be killed. Therefore, the PI controller is considered to be more practical in this experiment.

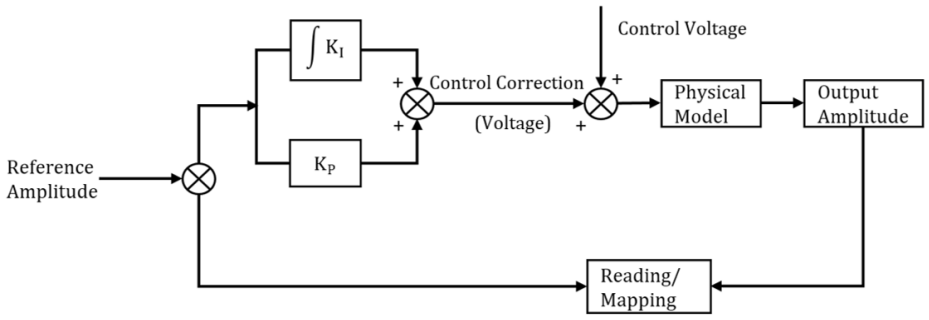

Figure 4.1: PI control

4.3 Control Implementation

As is shown in figure 4.1, there is a reference amplitude working as the set-point for the controlled variable (vibration amplitude) and an initial control voltage working as the reference of control value. The initial control helps the controller to reach a more smooth and stable transition and also decreases the settling time. It doesn't need to be too precise for the controller works strongly and accurately enough.

Since our controlled variable is exactly the vibration amplitude, and the amplitude reflects as the voltage in measurement from the sensor, we need to convert either the control goal to voltage in sensor reading, or the sensor data to displacement. We choose the latter one for its convenience to tuning. There is an empirical mapping formula in the loop, which is from sensor's calibration.

For the parameters Ki and Kp in the controller, we did several manual tuning and ended up with a series set of satisfying solutions with different working frequency ranges.

As in the software interface, we choose NI Labview to be the environment for its ability to read/write in loops simultaneously, and National Instrument's devices' high updating rate. From the view of the data acquisition port, there are two loops for reading and writing. Due to some updating overlap issues happened initially, we didn't put them in the same loop.

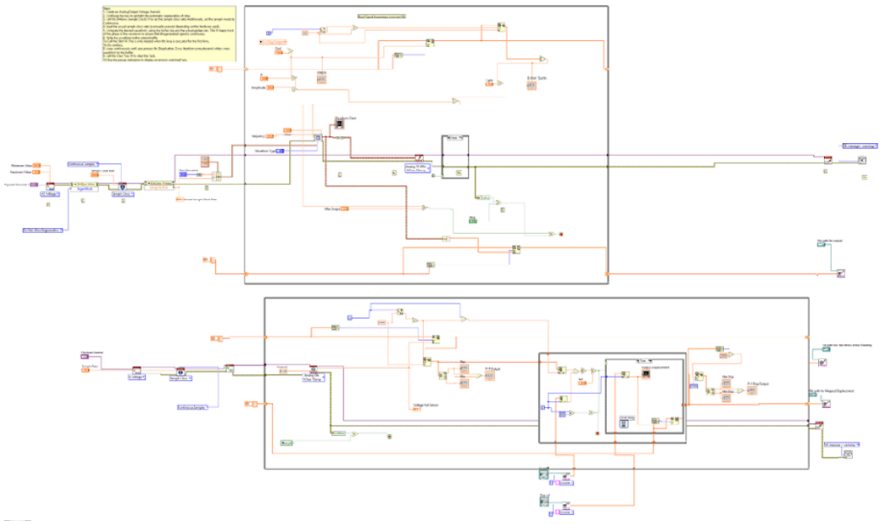

Figure 4.2: The control implementation in LabVIEW

In the reading loop, it reads 500 points, finds the maximum/minimum values among those points, calculates and stores the difference between the maximum and minimum points in each "big loop". Then after 20 "big loops", it takes the average from the stored differences to avoid random peak errors. The buffer number will change as the frequency changes to better adapt the algorithm.

In the writing loop, it also uses changing buffer number in different frequencies. Since the error calculation part is written in the writing loop, it takes another average in every 100 stored errors. Then this "averaged error" will be stored for another 100 times to calculate the "cumulative error" for the integral controller use. At the same time, the "averaged error" is used to implement proportional control.

Working together, those two loops read displacement data, realize PI control, and write control signals to the system.

Chapter 5

Testing

5.1 Setup

As is shown in the figure below, the main devices of the system are: a NI USB DAQ works as the communication port to generate control signals/ receive sensor measurement data, an audio amplifier works to enlarge the control signal enough to power the vibrator up, a subwoofer-based vibrator works to transfer given electrical signals to robust mechanical vibrations, and a hall effect sensor to detect the real-time position of the vibrator. Also, we fixed a high-speed camera to take videos of the end effector. In this experiment setup, we need to input required vibration amplitude and frequency in the PC interface, let the system generate vibrations and check the shaker's performance through high-speed videos/ displacement sensor reading.

5.2 Hall-effect sensor calibration

In our experiment, we are using a displacement sensor with a manually built board. The hall effect sensor is the DRV5053 Analog-Bipolar Hall Effect Sensor from Texas Instruments. It has a high sensitivity of up to 90 mV/mT [12], which is satisfied with our

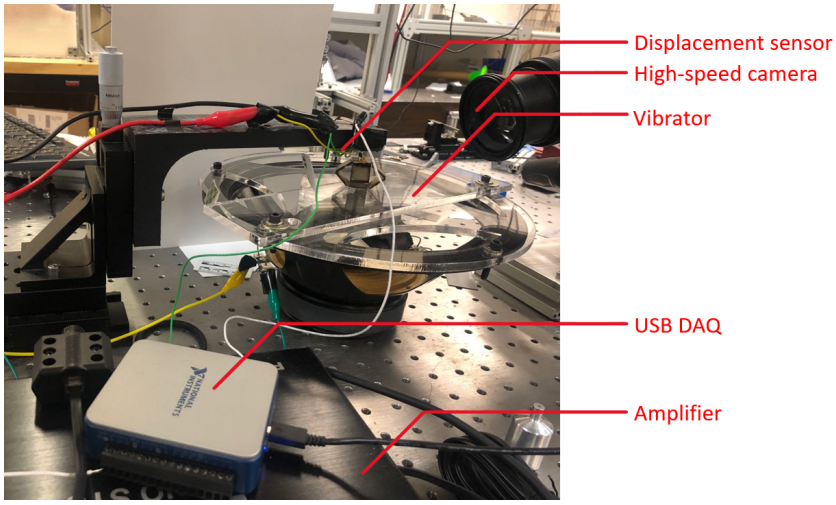

Figure 5.1: The experiment setup

application. To generate the required magnetic field, a small magnet is attached to the Sarrus linkage, and the hall effect sensor(along with the wired breadboard) was fixed to a linear moving stage as shown in figure 5.2. After testing and adjusting, the sensor setup has the ability to provide 0-1V voltage signal when the shaker vibrates in a range (1-4mm peak to peak) of amplitude.

After the tests, we fixed the whole experiment setup firmly, for the sensor's calibration will be influenced if there's anything moved even slightly. Because the hall effect sensor is fixed to a stage which could be operated precisely, we keep the shaker still and moved the sensor up and down slowly. During the manual operation, the vertical positions are recorded. Thus, an empirical calibration plot is given in figure 5.3, which indicates the relationship between the position and the output signal from the sensor. A 10-order curve fitting has been applied to provide more mapping points. It is also shown in figure 5.3, and we are going to use the fitted curve to be the mapping reference later.

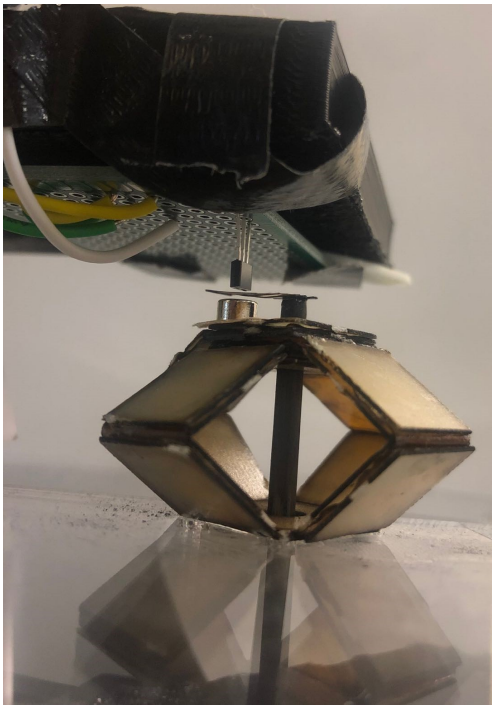

Figure 5.2: The displacement sensor setup

5.3 Open-Loop control performance

First, we tested the shakers performance with no sensor attended. The tests are done across a frequency range of 20Hz-150Hz. For each fixed frequency, we ramp the control amplitude up from tiny to apparent (approximately 0.1-2mm peak to peak amplitude) vibration.

5.3.1 Output tests in frequency sweep and amplitude sweep

For the raw data, we record the sensor's original output voltage. Figure 5.4 is an example of the data at 60Hz. As the control voltage ramps up, the sensor output voltage ramps up. There is a short oscillation at the beginning of the signal, the vibration shock's amplitude is not too big, and it turned stable quickly. It is easy to find that the curve is asymmetric due to the hall effect sensor's non-linear performance shown in the calibration

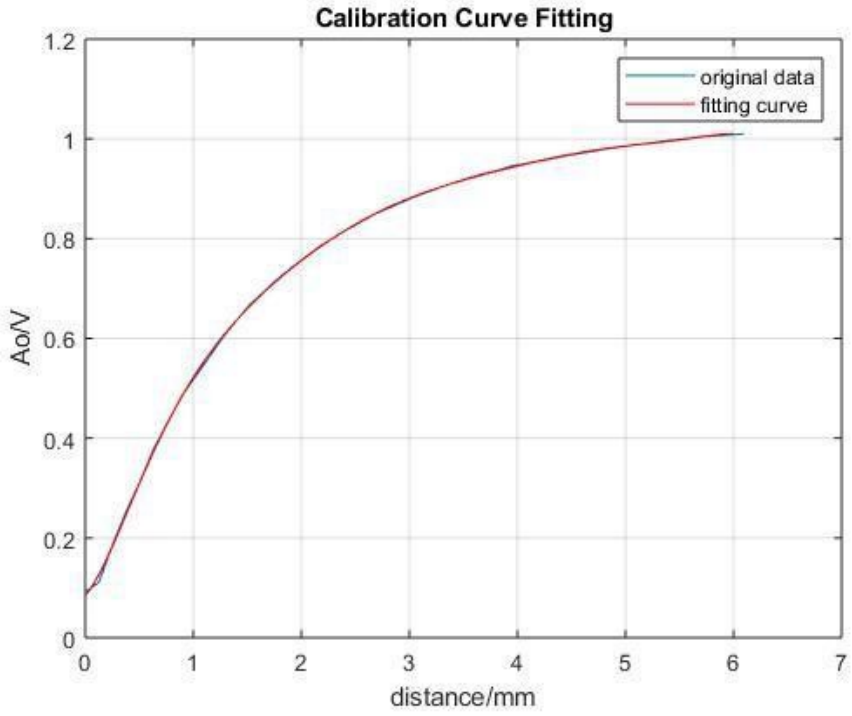

Figure 5.3: The calibration of the displacement sensor

result in figure 5.3.

Thus, we mapped the raw data using the empirical calibration result. As is shown in figure 5.4, the whole curve turned to be symmetric. Also, we can also tell from the zoom-in plot in figure 5.4, and the shaker is generating the smooth, steady, and accurate sinusoidal wave. A sinusoidal curve fitting has been applied, and the fitting error is in the acceptable range. Figure 5.4 is the shaker's performance at a specific frequency (60Hz), while the performances are all similarly good at other frequencies.

5.3.2 Fixed output target experiment

Now that the platform has proved its ability to generate a clean and smooth sinusoidal wave, we also need to find an empirical formula to control the vibration amplitude. It is clear reported from the previous sensor reading that the vibration amplitude increases

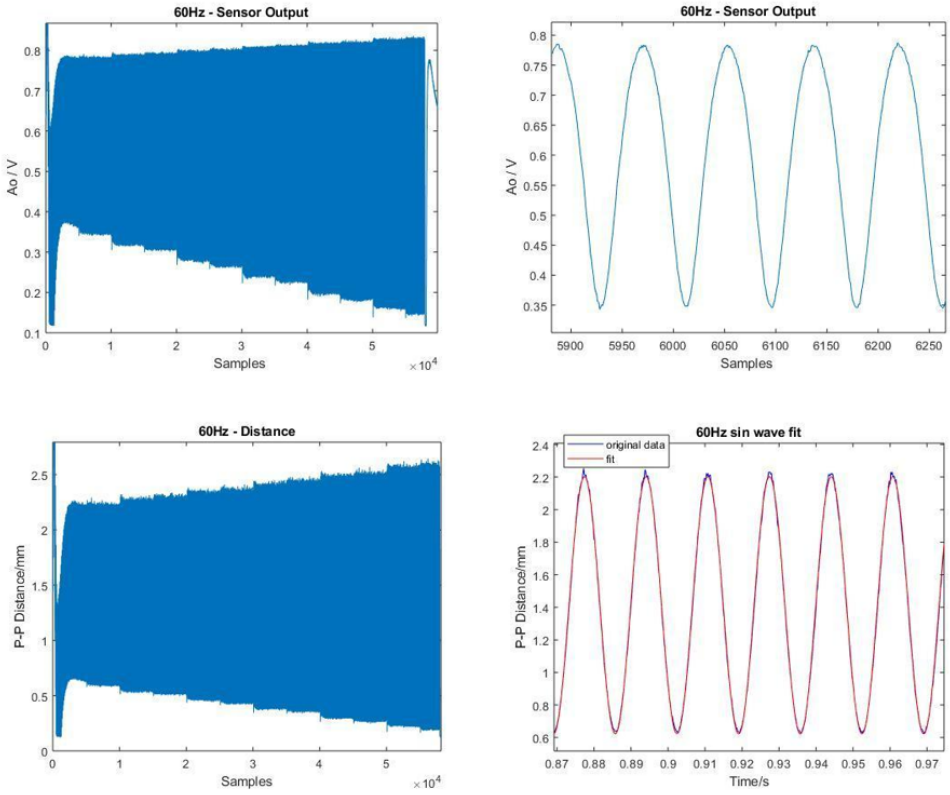

Figure 5.4: The output displacement data and zoom-in curves

when control voltage increases, and it is useful to sweep the control voltages across the frequency range.

As is shown in figure 5.5, we ramped up the control voltage with 20 30 samples for each frequency (from the left to the right, 10Hz -150Hz), and the voltage ramps provide vibrations with 0-2mm peak to peak amplitudes. Linear curve fittings have been applied to each amplitude sweep.

With the fitted empirical control voltage - output vibration peak-to-peak amplitude gain relationship, it is thus possible to control the platform to generate sinusoidal waves with a specific amplitude across all frequencies. In our test, we choose the 1mm peak-to-peak amplitude to be the control goal. Mapped from the empirical gain relationship, the 1mm-goal control result is shown in figure 5.6. The test is automatically done by the

program, with ramping up frequencies from 10Hz to 150Hz.

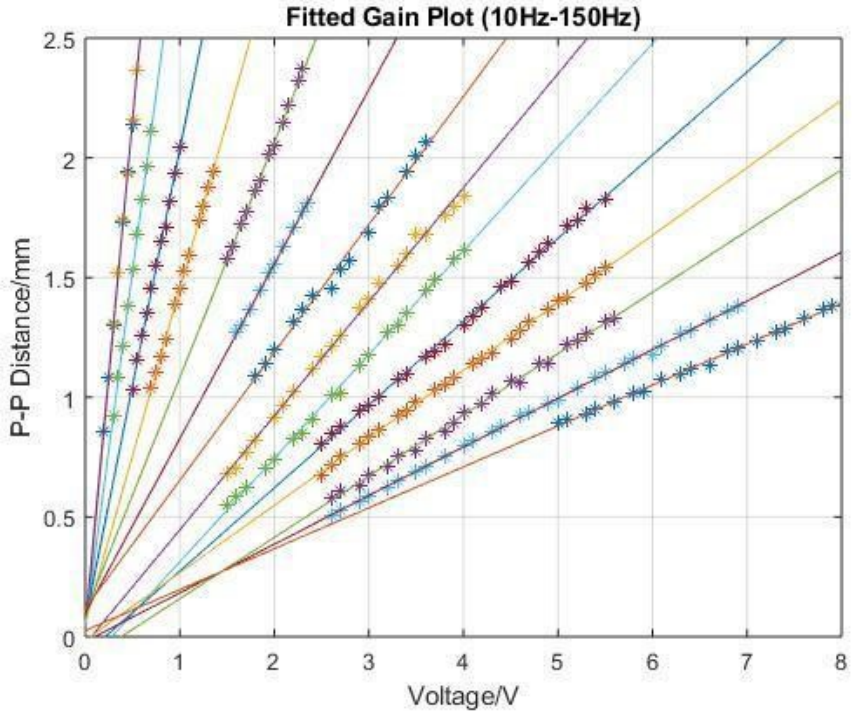

Figure 5.5: The empirical output-input gain plot

There are some reasonable peaks existed at points where frequency changed, and the output amplitude is basically around our 1mm goal. However, the system's performances are not detailed enough. For micro-robot application, an open-loop system is incapable to generate a satisfying sinusoidal wave with accurate amplitude. Therefore, a closed loop control is necessary for this vibration generating platform.

5.4 Closed-Loop control performance

5.4.1 Fixed output target experiment

We implemented a PI control in the system following the block diagram shown above in chapter 4. In general, it is the parameters tuning, which is the most challenging part

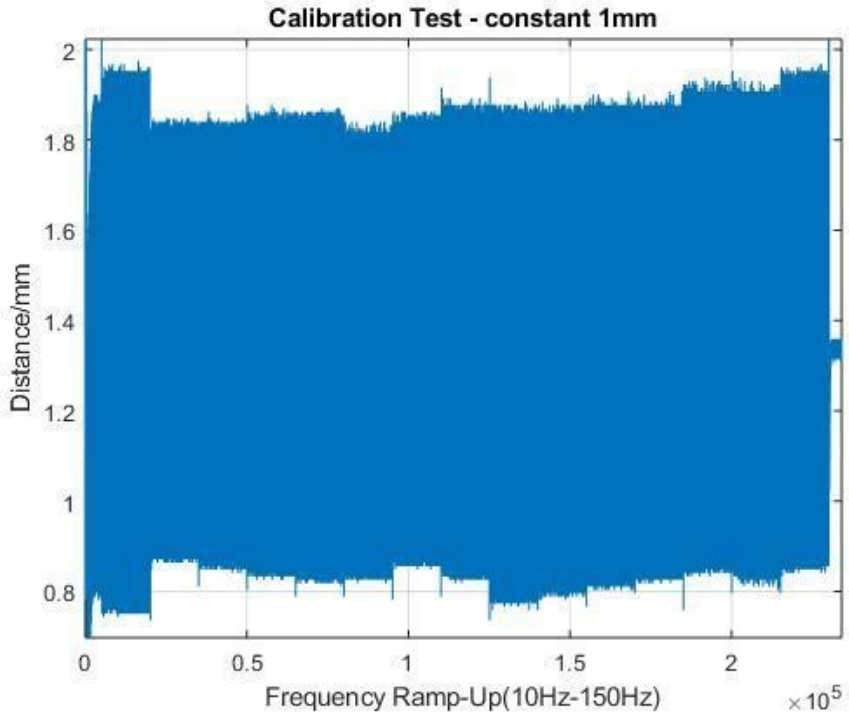

Figure 5.6: The fixed output(1mm) test result

in a PID controller. After realizing it is hard to find a satisfying parameters combination across all frequencies, we separate frequencies into different groups and find a series of parameters combinations. In details, they are:

Frequencies: 10Hz - 50Hz

Kp = 0.1

Ki = 0.03

Frequencies: 60Hz - 100Hz

Kp = 1

Ki = 0.08

Frequencies: 110Hz - 150Hz

Kp = 3

Ki = 0.15

Considering the relatively large working frequency range, it makes sense that we

have different satisfied parameters combination. For higher frequency, the proportional gain should be larger to achieve faster and stronger control correction.

Figure 5.7 shows the test results of the vibration platform integrated with closed-loop control. To better show the performances, we give both the control voltage adjusted automatically by the controller and the output vibration amplitude data from the sensor. A 1 mm peak-to-peak amplitude vibration is the control goal for the tests shown below.

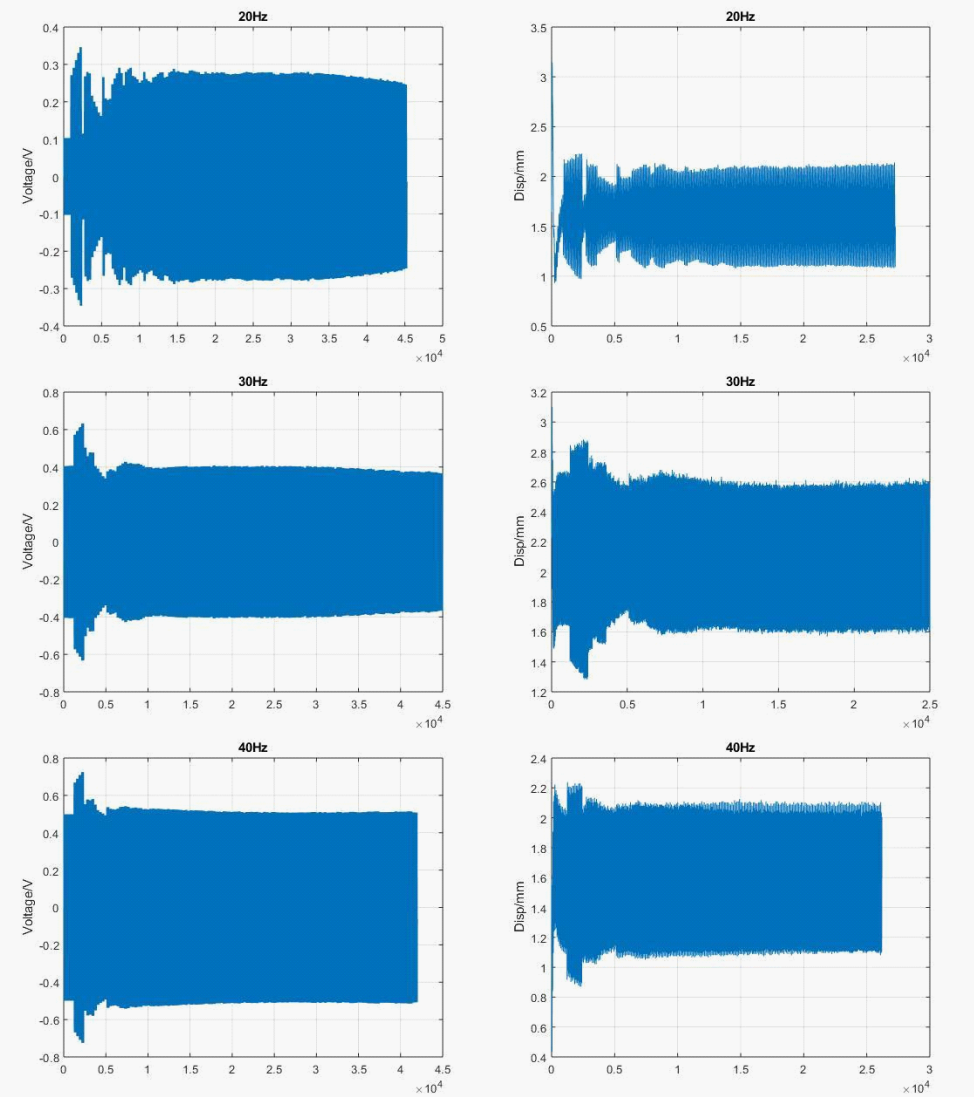

Figure 5.7: The control voltage and output displacement when no load added

Figure 5.7: continued

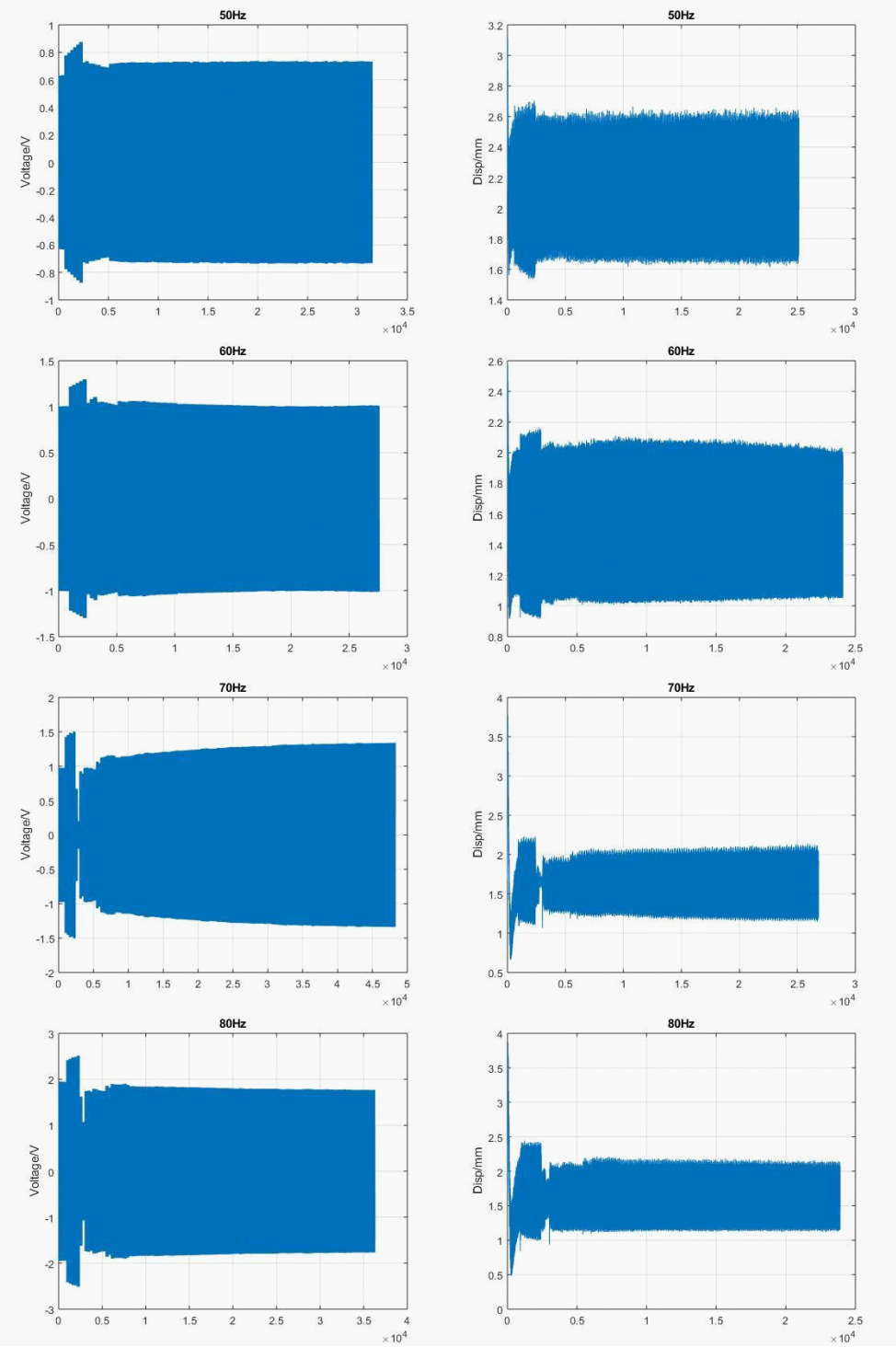

Figure 5.7: continued

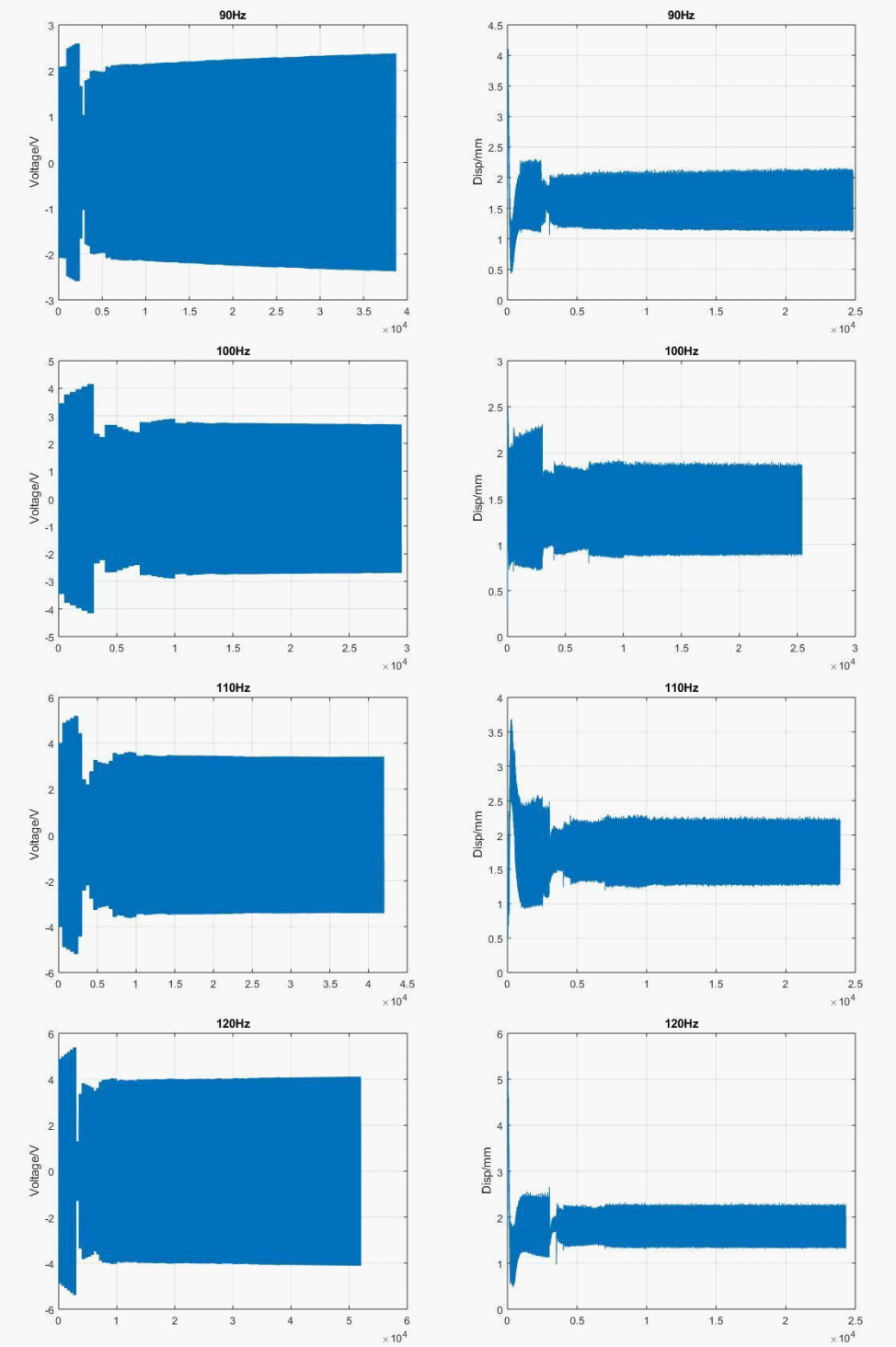

Figure 5.7: continued

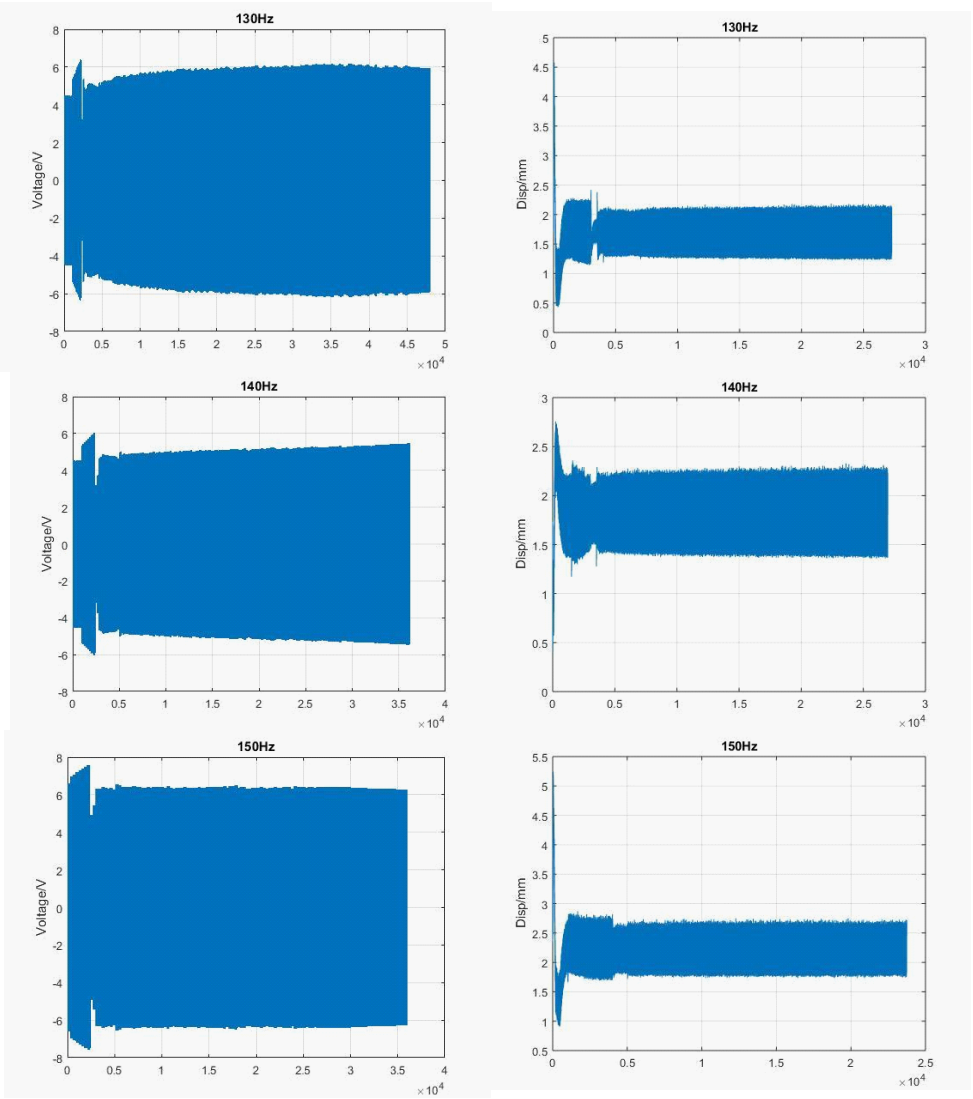

As is shown in the plots, the amplitude control transition has been realized quickly and smoothly. Although there are some slight oscillations and initial peaks, their influences are in acceptable range (oscillation amplitude is less than 1.5 mm) and won't damage the actuated micro-robot systems.

5.4.2 Load attached experiment

Now with the vibration platform which is capable to generate a steady clean sinusoidal wave, and the controller which is proved to work efficiently and accurately, we need to integrate the platform into real experiments to test the system's ability. Thus, we attached a micro wing to the carbon fiber rod to simulate the test scene in the micro aerial vehicle dynamics investigation. The micro wing, made by carbon fiber and Kapton film through lamination method, has the same size scale and weight scale as the Harvard Robobee (reference). It also has a compliant component parallel to the yaw direction, which could bring more complicated air dynamics in the system. As our goal for the platform is a reliable power source, which can resist all kinds of dynamic influences brought by actuated micro-robot systems, it needs to be able to generate the same accurate desired vibration when actuated micro-robot attended. It is sufficient to believe this micro wing part, along with the strong air drag force influences, could be evidence to show the vibration platform's ability to generate steady and robust actuating power in micro-robot system in this scale.

With the micro-wing attached, we set the output amplitude goal as the same 1 mm peak-to-peak and the controller parameters as the same as previously showed. We test the platform-wing system across the same frequency range (10Hz - 150Hz). The experimental setup is shown in figure 5.1, and the control voltage/ output vibration amplitude results are shown in figure 5.8.

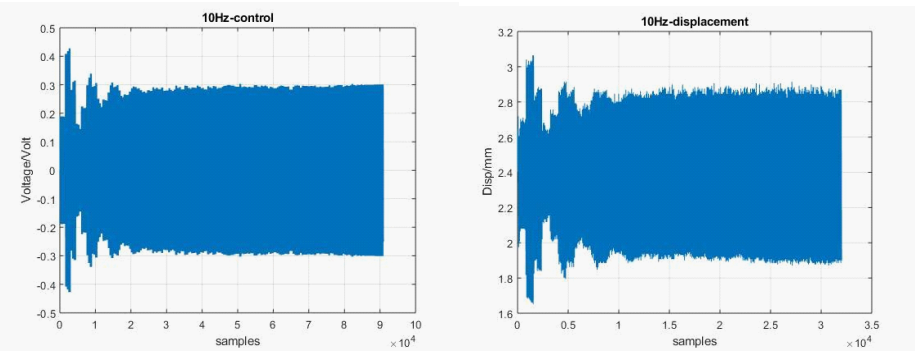

Figure 5.8: The control voltage and output displacement with the wing attached

Figure 5.8: continued

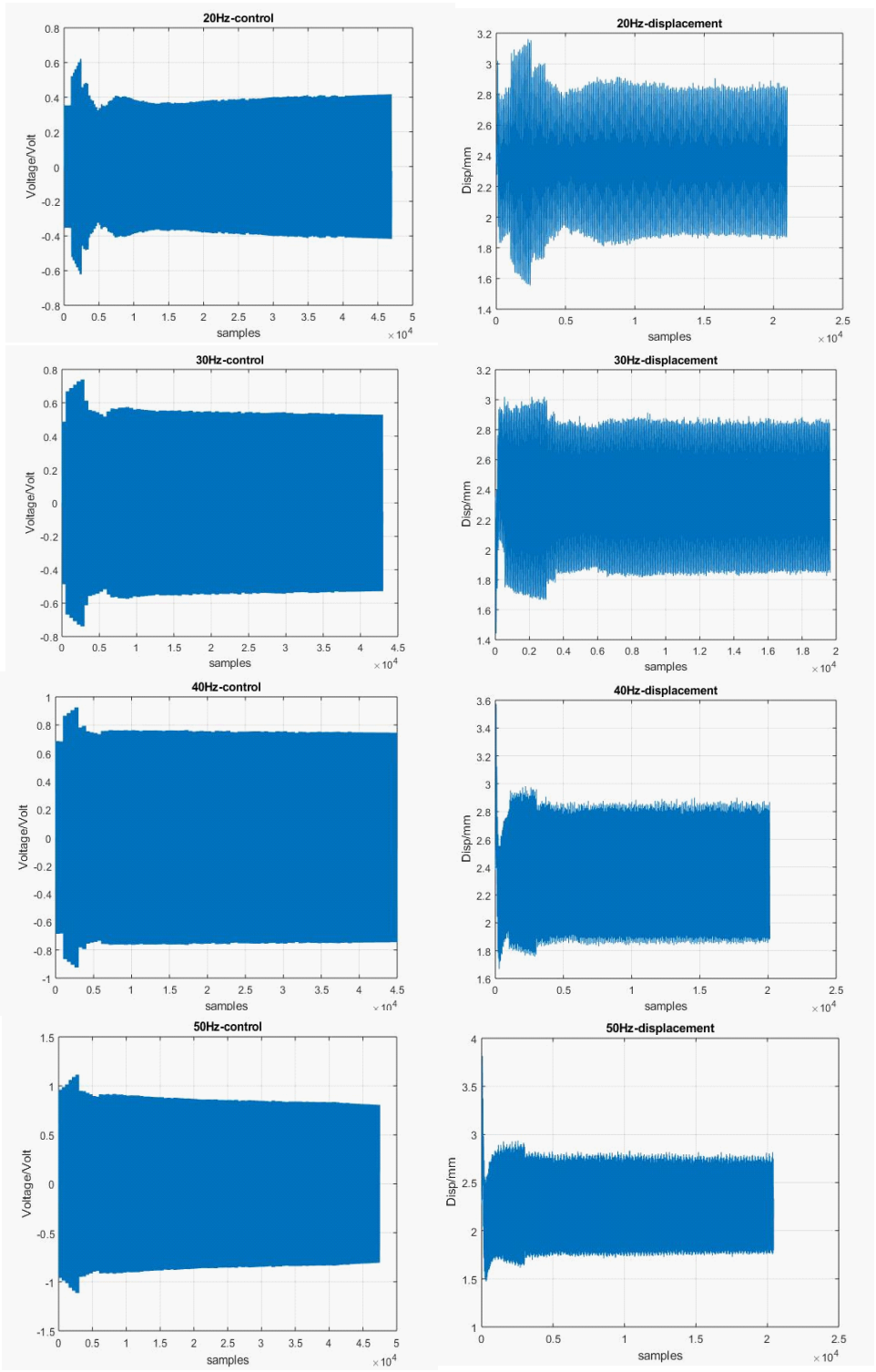

Figure 5.8: continued

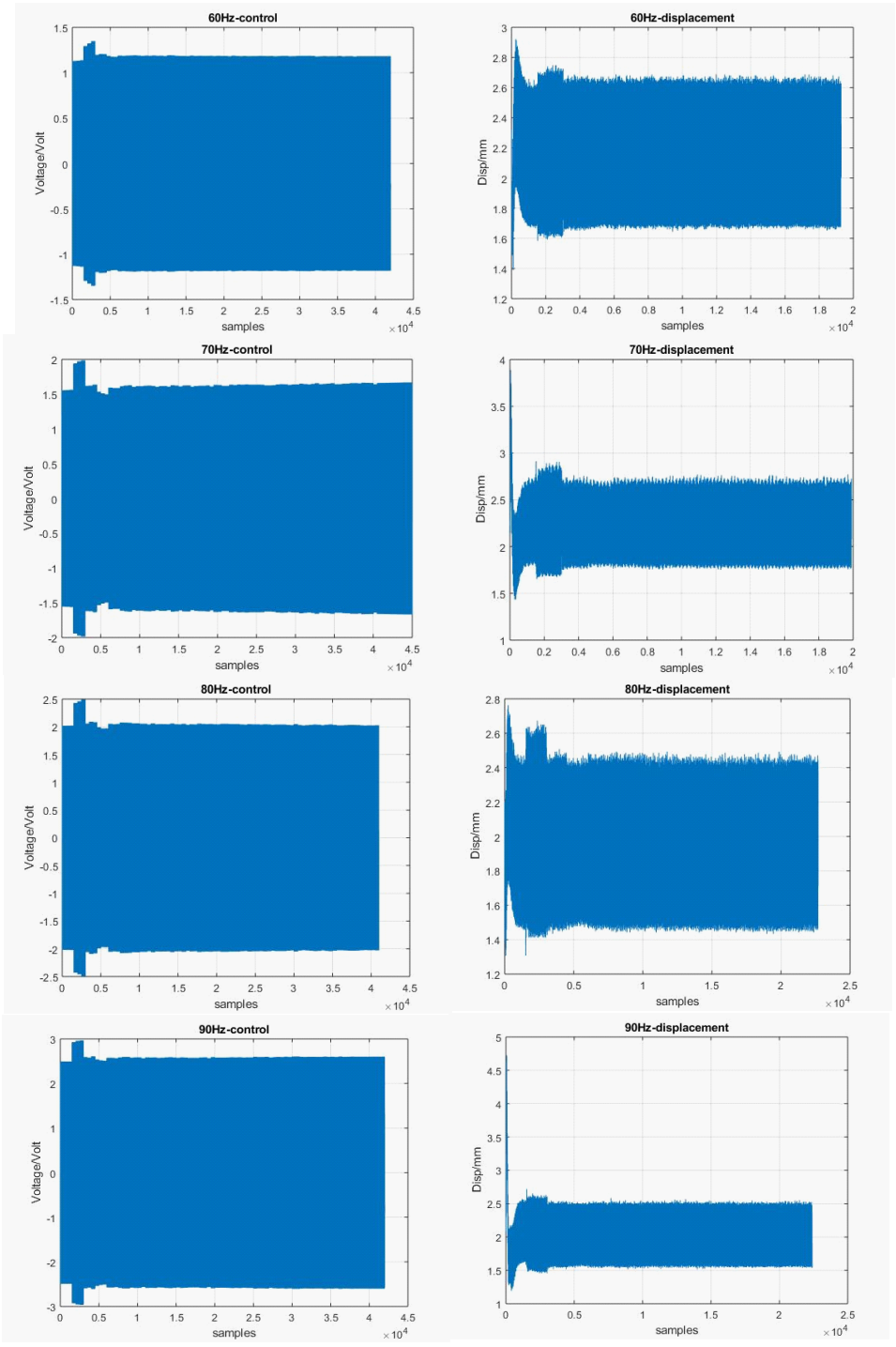

Figure 5.8: continued

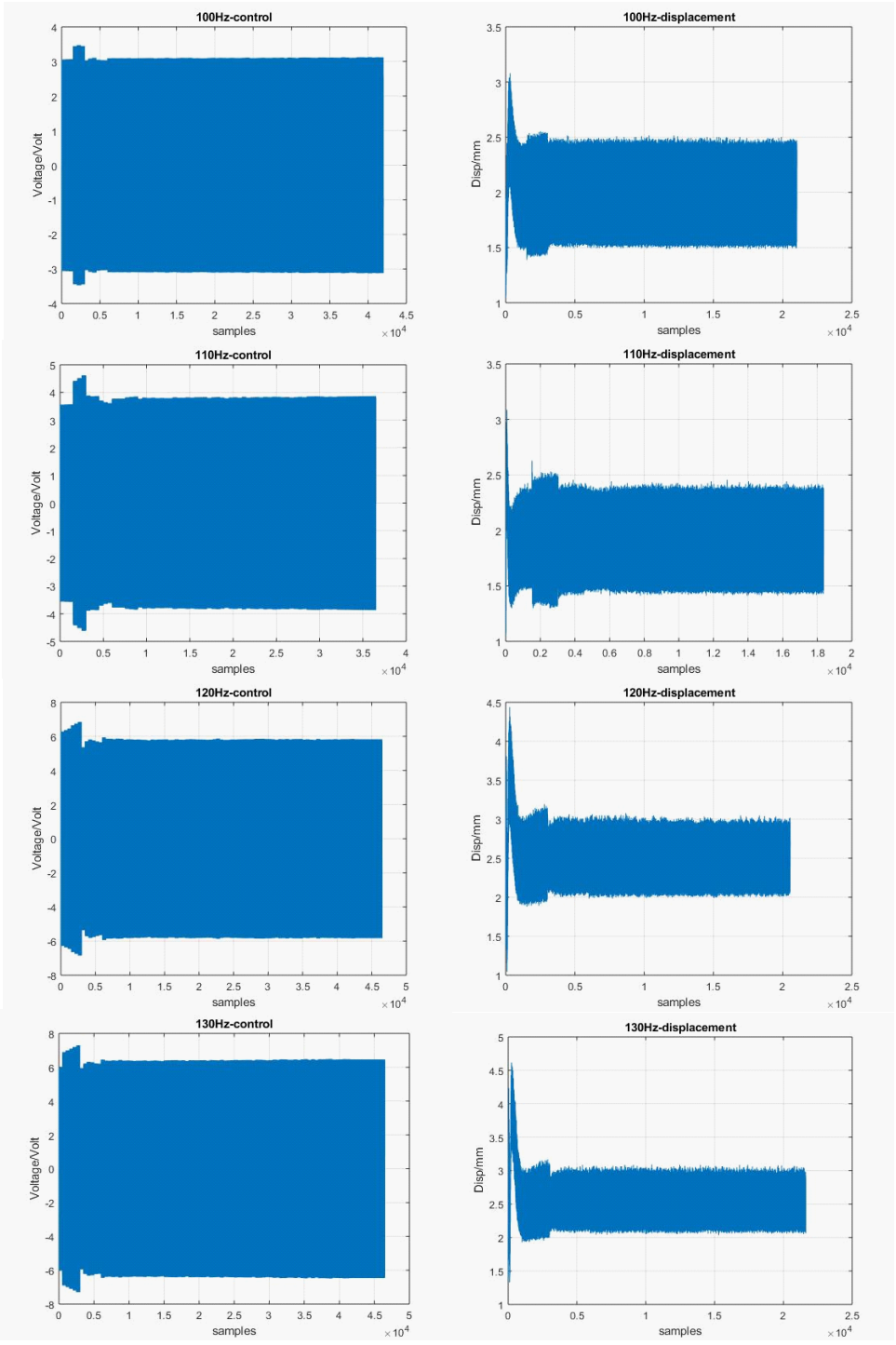

Figure 5.8: continued

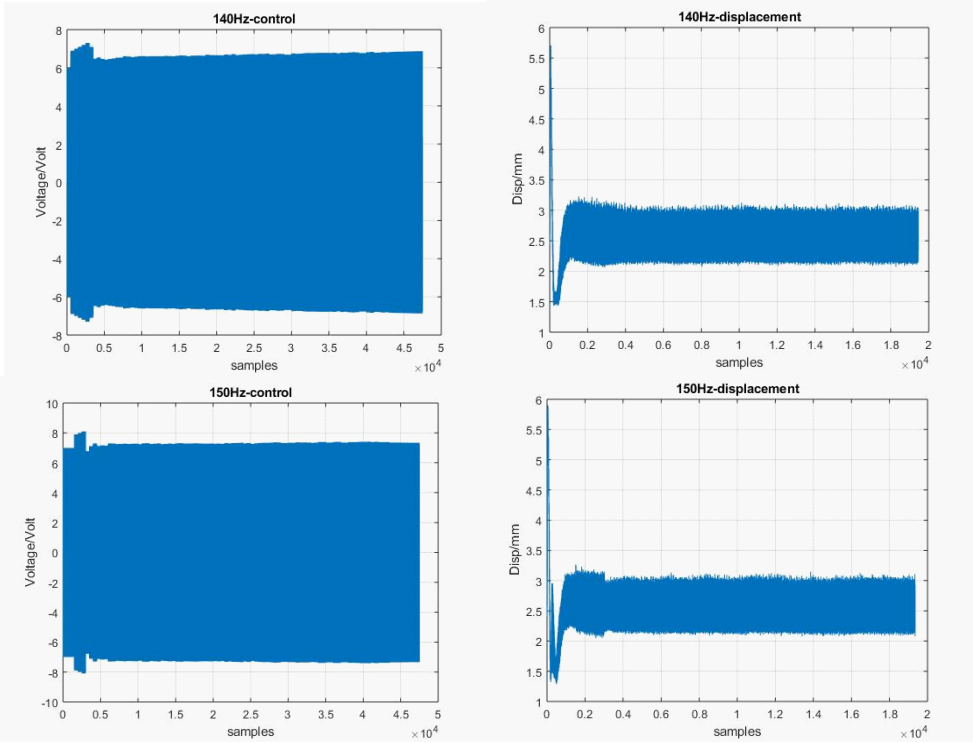

From the data shown above, there are no significant differences in the performances between two setups: a shaker platform without load, and a shaker platform with a micro-wing attached. All data are showing that the platform has the ability to generate accurate, stable and smooth-transition sinusoidal wave with a desired amplitude as required. To show the results in a clearer way, we take the last one-third steady period from the output displacement out, calculate the average amplitude, and obtain the error between the desired 1 mm goal and the real vibration. We repeat the error calculation for each frequency in both no wings attended, and wings attached, and plot them in figure 5.9 below.

As is shown in the error comparison plot above, the red line represents the error when no wings attended, and the blue line represents the error when the wings attached. All error points lay in a 0.05 mm absolute value from the data shown above, which is small enough to ignore. There is also no significant difference between the two error sets. Thus,

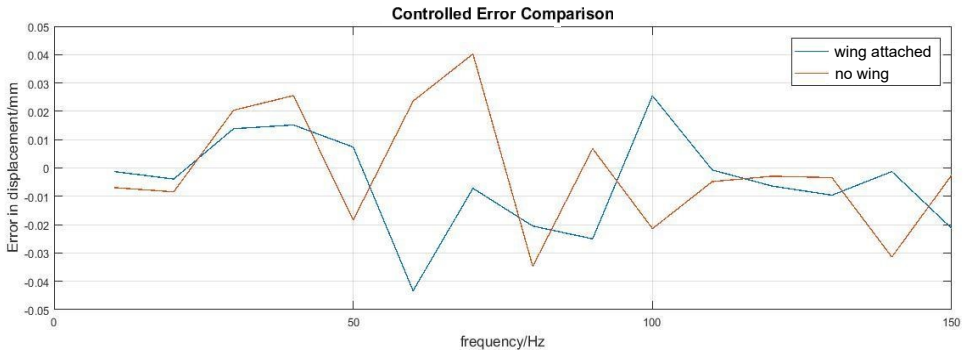

Figure 5.9: The error comparison

the vibration platform has proved to be reliable for generating controllable sinusoidal wave as the power source in micro robot studies at this scale.

Chapter 6

Conclusion and Future Work

6.1 Conclusion

Based on the voice coil idea, a vibration platform has been introduced. The vibration source includes a 10" subwoofer, a carbon fiber rod, an acrylic constraint board, and a Sarrus linkage. A micro wing was fabricated to test the platform's performance. Both the Sarrus linkage and the wing were designed and built using the SCM method to ensure accuracy and symmetry. Having a PI closed-loop controller, a PC control interface has been developed in LabView. In the tests, we measured the output displacement using a hall effect sensor. Also, we used a high-speed camera to take slow-motion videos to record detailed information.

In open loop control, the vibration platform has proved to generate an accurate and stable sinusoidal wave with peak-to-peak amplitude from 0.5mm to 2.5mm, 10 Hz to 150 Hz. From the frequency/amplitude sweep, we obtained an empirical gain relationship between the driving voltage and output vibration amplitude. Using the gain guide, the system was tested to generate a 1mm peak-to-peak amplitude sinusoidal wave with frequency ramping up. In general, it generated good desired signals with smooth transitions. However, the

errors from the open loop system are not ignorable and there is also a neutral position drift.

After tuning the parameters of the PI controller, we tested the vibration system for a 1mm peak-to-peak amplitude sinusoidal setpoint. From the control voltage data and the output displacement data, we found the system worked well to generate the desired goal. The settling times are short, and the transitions are smooth. No significant peaks appear to bring potential damages. To test the load capacity of the vibration system, a micro wing was attached to the carbon fiber rod (as the end effector). With the wing as the robot being tested, we used the same parameters set for the controller and tested with the same setpoint (1mm peak-to-peak amplitude). The system with the air dynamics load from the micro wing is still capable of generating stable and reliable vibration. We compared the errors at each frequency, in which the error is defined as the absolute difference between the set goal and the real output. All errors are lower than 0.05 mm, which is small enough to ignore. Also, there is no significant difference between no load applied and wing attached, and the platform is able to resist dynamics load at micro robot scale. Thus, we have successfully demonstrated a vibration platform which can be used as a robust, stable, and reliable testing power source in micro robot studies.

6.2 Future Work

In more complicated micro robot, it is often needed that the frequency changes when there is sudden motion (e.g., sharp turnings). Although the vibration platform demonstrated in this thesis is capable to generate accurate, reliable high-frequency wave, we only tested the system performance with output amplitude controlled at fixed output frequencies. The potential next step for this testing platform is to control the frequency and the vibration amplitude at the same time. The vibration platform will be able to

generate a series of accurate signals with different frequencies and amplitudes continuously. In that case, more complicated micro robot dynamics could be studied with this power solution.

Bibliography

[1] B. Aksak, M. P. Murphy, and M. Sitti. Gecko inspired micro-fibrillar adhesives for wall climbing robots on micro/nanoscale rough surfaces. In *2008 IEEE International Conference on Robotics and Automation*, pages 3058–3063. IEEE, 2008.

[2] A. T. Baisch, P. S. Sreetharan, and R. J. Wood. Biologically-inspired locomotion of a 2g hexapod robot. In *2010 IEEE/RSJ International Conference on Intelligent Robots and Systems*, pages 5360–5365. IEEE, 2010.

[3] A. T. Baisch and R. J. Wood. Pop-up assembly of a quadrupedal ambulatory microrobot. In *2013 IEEE/RSJ International Conference on Intelligent Robots and Systems*, pages 1518–1524. IEEE, 2013.

[4] S. Chopra. *Piezoelectric Actuators with Embedded Strain Sensors for Micro Robotic Applications*. University of California, San Diego, 2018.

[5] L. W. Cockrum and C. Kline. Subwoofer speaker system, Sept. 15 1992. US Patent 5,147,986.

[6] N. W. Hagood, W. H. Chung, and A. Von Flotow. Modelling of piezoelectric actuator dynamics for active structural control. *Journal of intelligent material systems and structures*, 1(3):327–354, 1990.

[7] E. W. Hawkes and D. Lentink. Fruit fly scale robots can hover longer with flapping wings than with spinning wings. *Journal of the Royal Society Interface*, 13(123):20160730, 2016.

[8] T. Ho, S. Choi, and S. Lee. Development of a biomimetic quadruped robot. *Journal of Bionic Engineering*, 4(4):193–199, 2007.

[9] T. Honda, K. Arai, and K. Ishiyama. Micro swimming mechanisms propelled by external magnetic fields. *IEEE Transactions on Magnetics*, 32(5):5085–5087, 1996.

[10] G. Inc. https://glowforge.com/our-products.

[11] M. Inc. http://www.moticont.com/sdlm-025-070-01-01.htm.

[12] T. Instruments. http://www.ti.com/lit/ds/symlink/drv5053.pdf.

[13] N. T. Jafferis, M. A. Graule, and R. J. Wood. Non-linear resonance modeling and system design improvements for underactuated flapping-wing vehicles. In *2016 IEEE International Conference on Robotics and Automation (ICRA)*, pages 3234–3241. IEEE, 2016.

[14] K. Jones, C. Bradshaw, J. Papadopoulos, and M. Platzer. Bio-inspired design of flapping-wing micro air vehicles. *The Aeronautical Journal*, 109(1098):385–393, 2005.

[15] B. Kim, M. G. Lee, Y. P. Lee, Y. Kim, and G. Lee. An earthworm-like micro robot using shape memory alloy actuator. *Sensors and Actuators A: Physical*, 125(2):429–437, 2006.

[16] J. Kim, H.-K. Kim, and S.-B. Choi. A hybrid inchworm linear motor. *Mechatronics*, 12(4):525–542, 2002.

[17] R. Le Letty, F. Claeyssen, F. Barillot, M. F. Six, and P. Bouchilloux. New linear piezomotors for high-force precise positioning applications. In *Smart Structures and Materials 1998: Smart Structures and Integrated Systems*, volume 3329, pages 748–756. International Society for Optics and Photonics, 1998.

[18] D. Lentink, S. R. Jongerius, and N. L. Bradshaw. The scalable design of flapping micro-air vehicles inspired by insect flight. In *Flying insects and robots*, pages 185–205. Springer, 2009.

[19] K. Y. Ma, P. Chirarattananon, S. B. Fuller, and R. J. Wood. Controlled flight of a biologically inspired, insect-scale robot. *Science*, 340(6132):603–607, 2013.

[20] K. Y. Ma, S. M. Felton, and R. J. Wood. Design, fabrication, and modeling of the split actuator microrobotic bee. In *2012 IEEE/RSJ International Conference on Intelligent Robots and Systems*, pages 1133–1140. IEEE, 2012.

[21] S. Mori, M. Furuya, A. Naganawa, Y. Shibuya, G. Obinata, and K. Ouchi. Nano-motion actuator with large working distance for precise track following. *Microsystem technologies*, 13(8-10):873–881, 2007.

[22] S. Mori, T. Hoshino, G. Obinata, and K. Ouchi. Air-bearing linear actuator for highly precise tracking. *IEEE transactions on magnetics*, 39(2):812–818, 2003.

[23] K. Oldham, J. Pulskamp, R. Polcawich, P. Ranade, and M. Dubey. Thin-film piezoelectric actuators for bio-inspired micro-robotic applications. *Integrated Ferroelectrics*, 95(1):54–65, 2007.

[24] C. Ruffert, R. Gehrking, B. Ponick, and H. H. Gatzen. Magnetic levitation assisted guide for a linear micro-actuator. *IEEE transactions on magnetics*, 42(11):3785–3787, 2006.

[25] F. Z. Temel and S. Yesilyurt. Magnetically actuated micro swimming of bio-inspired robots in mini channels. In *2011 IEEE International Conference on Mechatronics*, pages 342–347. IEEE, 2011.

[26] K. Uchino. *Piezoelectric actuators and ultrasonic motors*, volume 1. Springer Science & Business Media, 1996.

[27] Z. Wang, G. Hang, J. Li, Y. Wang, and K. Xiao. A micro-robot fish with embedded sma wire actuated flexible biomimetic fin. *Sensors and Actuators A: Physical*, 144(2):354–360, 2008.

[28] Wikipedia. https://en.wikipedia.org/wiki/fr4.

[29] Wikipedia. https://en.wikipedia.org/wiki/kapton.

[30] Wikipedia. https://en.wikipedia.org/wiki/sarrus$_l$*inkage*.